PHOSPHATE CYCLING IN THE PRESENCE OF BIOGENIC IRON OXIDES AND IRON-REDUCING BACTERIA

A THESIS
SUBMITTED TO THE INSTITUTE OF THE ENVIRONMENT
OF THE UNIVERSITY OF OTTAWA
IN PARTIAL FULFILLMENT OF THE REQUIREMENTS
FOR THE DEGREE OF
MASTER OF SCIENCE

by

EMILY MEYERS

August 2017

Abstract

Nutrient pollution from industrial activity is an environmental problem that persists in water bodies near urban settings, and has been a primary contributor to eutrophication, bacterial contamination, and harmful algal blooms. Biogenic iron oxides offer a potential solution to the treatment of lakes and rivers containing high concentrations of phosphate, the limiting nutrient in aquatic systems. Soluble ferrous iron can act as an electron donor for iron-oxidizing bacteria, which thrive in low-oxygen environments. This results in the formation of insoluble ferric iron minerals, ideal adsorbents for negatively charged phosphate. Conversely, iron-reducing bacteria reduce ferric iron to form ferrous iron, resulting in the formation of secondary minerals depending on the chemistry of the particular environment.

This project investigates the chemical conditions at which biogenic iron oxides have the maximum adsorptive capacity, especially with respect to organic carbon content. A simplified model of natural biogenic iron oxides was synthesized by co-precipitating the mineral ferrihydrite (a common iron oxide) with the polysaccharide alginate, an analogue to bacterial exopolysaccharides. At the levels of carbon investigated, organic matter was not found to affect the adsorptive capacity of iron oxides at the C/Fe ratios analyzed. Similarly, organic matter did not appear to significantly influence the rate of reduction of ferrihydrite by the iron-reducing bacterium *Shewanella putrefaciens* CN32. Presence of organics did however influence rates of reduction and the mineralogy of the post-reduction precipitates. Phosphate adsorbed to iron oxides prior to microbial reduction greatly increased both the rate and the extent of ferric iron reduced, and also had an impact on the secondary minerals that formed (vivianite, green rust).

An improved understanding of these conditions could contribute to a more efficient process by which iron-oxidizing bacteria are used for large-scale industrial water treatment.

Résumé

La pollution causée par les nutriments provenant d'activités industrielles est un problème environnemental présent dans plusieurs écosystèmes aquatiques. Cette pollution contribue à l'eutrophisation, à la contamination par les bactéries et à la prolifération d'algues toxiques. Les oxydes de fer biogéniques représentent une solution potentielle pour traiter les cours d'eau et les lacs contenant des concentrations excessives de phosphate, lequel est un élément limitant des écosystèmes d'eaux douces. Le fer ferreux soluble est un donneur d'électron pour les bactéries oxydantes du fer qui vivent en milieu peu oxygéné. Leur activité métabolique mène à la précipitation d'oxydes de fer ferrique insolubles lesquels peuvent agir comme excellent sorbant de phosphate soluble. Ces mêmes oxydes peuvent toutefois être réduits par des bactéries réductrices de fer en milieu anoxique ce qui entraine la formation de minéraux secondaires et la solubilisation des oxydes de fer.

Ce projet s'est intéressé à la sorption de phosphate sur d'oxydes de fer biogéniques ainsi qu'à l'effet du contenu en carbone organique des oxydes sur la capacité de sorption. Des oxydes de fer synthétiques on été préparés en co-précipitant de la ferrihydrite (un oxyde de fer commun) avec de l'alginate, lequel possède des propriétés chimiques similaires à celles des exo-polysaccarides des bactéries oxydantes du fer. Les concentrations de carbone organique utilisées dans cette étude n'ont pas affecté la sorption du phosphate sur les oxydes de fer synthétiques ainsi que leur réduction en présence de *Shewanella putrefaciens* CN32. La quantité et la présence de carbone organique dans les oxydes de fer a toutefois influencé les taux de réduction et la minéralogie des minéraux secondaires se formant à la fin de la réduction. La présence de phosphate pré-sorbé à la surface des oxydes de fer a causé une augmentation des taux de réduction et a mené à la formation de minéraux secondaires comme la vivianite et la rouille-verte.

Cette étude présente de nouveaux résultats pouvant être utilisés dans le design de systèmes de traitement d'eau avec des bactéries oxydantes du fer.

Acknowledgements

I would first like to thank my supervisor Dr. Danielle Fortin for her guidance and expertise throughout this process. She agreed to take me on as a student from a different department but still provided me with the same attention, encouragement, and quick email response time as her geochemistry students. I feel lucky to have worked under such a distinguished yet cheerful scholar.

Huge thanks to PhD candidate Maeve Moriarty for being my lab mom and friend throughout this past year and a half, who taught me everything from laboratory procedures to data analysis, and answered all my (mundane) questions. Your help, patience, and coaching are more appreciated than you know. Thank you to Tarek Najem for taking me through all the nitty-gritty details of carrying out some seriously complex lab work, who once even spent an entire Saturday in the lab with me to help set up my first reduction experiment. Your dedication to your research is impressive and very admirable. And thanks to Liz Ashby for giving me my first taste of fieldwork. Your positive attitude and practical advice make me wish that our lab time had overlapped more.

I certainly would not have made it through in once piece were it not for the unwavering support of my parents, Ghiselle & Rick, and my brother Warren. You have each set a tremendous example of what it means to work hard for something worthwhile. Your love and concern went a long way in pushing me through moments of uncertainty and frustration. Thank you guys for believing I could do this!

I am grateful to the hardworking staff at BIOTECanada for allowing me to stick around on a very part-time basis over the past 2 years. You know you've got a supportive corporate environment when coming into the office feels like home.

A big thank you to my dear friends who checked up on me throughout my research and pretended to be interested when I fretted about leaks in the anaerobic chamber and looming deadlines. Reassurance and occasional distraction was always provided when needed most. Last but not least, thanks to Adam Schoones for helping me keep my spirits up.

Table of Contents

List of Figures

List of Tables

1. Introduction

Phosphorus is a nutrient that is fundamental to all forms of life because of its role in the regulation of cellular processes. The preferred source of phosphorus for bacteria is phosphate, a polyatomic ion with a net charge of -3. In aquatic environments, it is often a limiting nutrient because of its presence in relatively low (nano- to micromolar range) concentrations (Jaisi 2011). Phosphorus cycling is intimately connected with geochemical cycling of other elements, notably iron (Romano 2017). In agricultural areas, excessive fertilizer application has released phosphate to surface waters, causing widespread ecological damage.

1.1 *Phosphate as a pollutant*

Phosphate pollution from industrial activity is an environmental problem that persists in many water bodies near urban settings, and has been a primary contributor to eutrophication, bacterial contamination, and harmful algal blooms. Phosphorus was banned from commercial detergents in the 1970s once it became known as a limiting factor in nutrient pollution, but it remains a common component of fertilizer along with nitrogen and potassium. Surface runoff from pastures and farms, combustion emissions, and septic tank discharges are some of the primary sources of nutrient pollution. Its widespread use in domestic and industrial practices has allowed phosphorus to persist as a pollutant in lakes, rivers, and oceans worldwide.

Aquatic nutrient pollution results in many damaging effects to ecosystems. Phosphorus is the main cause of eutrophication, a type of water pollution characterized by excessive enrichment of an ecosystem with nutrients (Schindler and Vallentyne 2004). This results in an overgrowth of organisms including as 'blooms' of phytoplankton. These increases in productivity can limit light to deeper layers of the water, which depletes aquatic environments of oxygen, resulting in hypoxia. Some algae produce toxins that can kill wildlife and render the water unsafe for human consumption and recreational activity (Lau et al. 1997). Shifts in species populations resulting from a sudden plant or bacterial overgrowth can throw off the food web balance. Algal blooms can also cause deficits in dissolved oxygen (Jackson and Lochmann 1992). Though also a natural

process, human activity greatly increases the rate at which phosphorus enters waterways.

Wastewater is an unavoidable byproduct of many current industrial processes. Often containing high concentrations of toxic chemicals and environmental pollutants, most governments have regulations in place that require wastewater to be treated before being released back into the environment, though these limits are not always strictly enforced. One of the most prominent sources of nutrients is runoff from farms and fields, coming from industrial fertilizers containing high amounts of phosphorus and nitrogen, and from livestock sewage. During the treatment of agro-industrial wastewater, these nutrients may be left in the water after filtration of solids because they are not toxic.

A review of phosphorus removal methods summarizes the main commercial processes in use for sequestration of excess phosphorus from wastewater (de-Bashan and Bashan 2004). The most common techniques are: constructed wetlands for nutrient control, phosphorus precipitation by metal salts, phosphate removal with cultured bacteria and microalgae, and enhanced biological phosphorus removal. Many of these are only being used at small scales for the purposes of improving the design and process. A key observation from this review is that the chemical precipitation of phosphate makes it challenging for it to be recycled and used for industrial purposes, emphasizing the potential for removing phosphate using biological methods. Phosphate removal from aquatic environments via biogenic iron oxides is therefore a valid topic to investigate. The review concludes by stating that further research is required to complete our understanding of effective and efficient phosphorus removal and recycling (de-Bashan and Bashan 2004).

1.2 *Iron minerals*

Iron is the most abundant element by mass on Earth, and the fourth most prevalent element in the Earth's crust (Schwertmann 1991). It plays a key role in the biogeochemical processes of soils and sediments. Iron's atomic structure makes it able to exist in many oxidation states, with +2 (ferrous) and +3 (ferric) being the most

common, making it very reactive. In particular, iron tends to react with air and water, forming rust and iron minerals, which make up close to 50% of the weight of soils (Jambor and Dutrizac 1998). These minerals can act as adsorbents for nutrients and pollutants since they often have reactive functional groups and substantial surface area (Cornell and Schwertmann 2003).

Iron oxides are compounds resulting from reactions between iron, oxygen and hydrogen. Iron oxyhydroxides also contain these components along with hydroxide groups, and are grouped with iron oxides as they share most properties (Cornell and Schwertmann 2003). Iron enters the environment as Fe(III) from the Earth's crust through weathering of rock, and can then be transformed to iron oxides via processes such as deprotonation, hydrolysis, crystallization, thermal transformation, hydration/ dehydration, oxidation, dissolution, and precipitation. Under oxic conditions at near neutral pH, Fe(II) is rapidly oxidized to Fe(III) and precipitates as solid iron oxide (Stumm and Morgan 1996). The majority of iron oxides can form minerals of well-defined crystal structure with a basic octahedral unit, where six O or OH groups encircle each iron atom. Each type of iron oxide primarily differs in the spatial organization of the $Fe(O,OH)_6$ octahedra. Different forms of iron oxides can readily interconvert, especially with changes in pH, Eh, temperature, pressure, water activity, and oxic/anoxic conditions (Schwertmann and Cornell 2000). Therefore, the presence of certain iron oxides can indicate the characteristics of their environment of formation.

The flux between Fe(II) and Fe(III) is of interest in environments such as soils that experience a great deal of reduction-oxidation (redox) activity. This variability can be attributed to changes in the availability of electron donors (i.e. an increase in organic carbon) and electron acceptors, such as dissolved oxygen. An understanding of these redox conditions and reactions is of key importance for determining iron mineralization pathways (Mejia et al. 2016). The formation of iron minerals in soils has an immediate impact on the availability of nutrients, the metabolic pathways of microbes, and the mobility of contaminants (Borch 2010), and is therefore of significant environmental importance.

In aerobic conditions, the iron oxide minerals hematite and goethite are the most stable in terms of thermodynamics, and as such, are the most abundant iron oxides found in soils. Many other iron oxides are also ubiquitous because their kinetics of formation are favourable, and the rate of transforming to stable arrangements is relatively slow (Straub 2001). Iron oxides that are found at surfaces are frequently defective and exhibit low crystallinity (Schwertmann and Cornell 2000). The reason for this is likely because they are formed at low temperatures in environments that contain a wide range of elements and compounds.

In anoxic environments, ferric minerals may undergo reduction and/or reductive dissolution via iron-reducing bacteria forming ferrous iron. Depending on the conditions, Fe(II) may remain in solution, precipitate as secondary minerals, or be re-oxidized to form new Fe(III) minerals (Konhauser 2011). These biogeochemical processes can progress either by abiotic or biotic means, the latter by iron-reducing bacteria such as those within the *Geobacter* and *Shewanella* genera.

Ferrihydrite is an amorphous, hydrous, ferric oxyhydroxide that is prevalent in aquatic environments and in soils. It can form under a variety of conditions including marine and freshwater areas, aquifers, sediments, and mine sites. It can only be found in nature as a very fine-grained nanomaterial and as such, its crystal structure has been difficult to identify and is still somewhat contentious (Rancourt and Meunier 2008, Manceau 2011). It is, however, known to be a hydrous ferric oxyhydroxide mineral and its framework is thought to contain layers of oxygen and hydroxide molecules (Barron and Torrent 2003). It occurs naturally in weathered iron-rich soils, especially those that contain significant amounts of dissolved silica and phosphate, which are known to adsorb to the mineral surface and prevent it from being converted to more crystalline iron minerals (Childs 1992). Ferrihydrite's large surface area and surface coordination properties make it an important mineral in the context of environment and remediation.

Ferrihydrite is still considered a mineral despite its poorly defined morphology and composition of nanoparticles. Using X-ray diffraction, ferrihydrite can be characterized by its broad peaks. Depending on how ordered it is, ferrihydrite can manifest in one of

two forms: either as 2-line ferrihydrite, which exhibits 2 broad peaks in its most disordered state, or six sharper peaks (6-line ferrihydrite) it its most crystalline state (Manceau and Drits 1993).

Ferrihydrite and other iron minerals are commonly found in nature in close association with organic matter (OM) (Carlson and Schwertmann 1981). Under certain conditions, dissolved OM and iron ions form co-precipitates, which can contain up to 10% carbon (McKnight et al. 1992). The organic matter in soils comes from decayed plant and animal matter and contains high levels of nutrients. The fraction of OM fraction in soils is referred to as humus, which produces the acidic mixtures humic acid and fulvic acid. The quantity and characteristics (i.e. pH, functional groups) of the OM in a particular location can vary greatly and create a wide range of conditions that have complex effects on geochemical processes. The influence of OM (alginate, a polysaccharide) co-precipitated with iron oxides on these natural processes will be examined in this study, and compared to pure ferrihydrite.

Iron oxides offer a potential solution to the treatment of aquatic environments that have a high concentration of phosphate (Emerson and de Vet 2015). The positive surface charge of iron and iron minerals makes them ideal adsorbents for phosphate, an anion with a charge of -3. The amount of phosphate that can be adsorbed per unit iron oxide is referred to as its adsorptive capacity. When anions such as phosphate are introduced to the system, they will theoretically displace outward-facing hydroxide ions and bond to the mineral particle surface. The influx of hydroxide ions into the bulk fluid therefore results in a predicted increase in pH during and after adsorption.

1.3 *Adsorption onto iron oxides*

When an adsorbent (i.e. solid iron) and an adsorbate such as aqueous phosphate are in contact for a sufficient amount of time, the system eventually reaches equilibrium, whereby phosphate molecules adsorb to iron and desorb to the bulk fluid at the same rate. This relationship can be described by a model called an adsorption isotherm that is adjusted to fit experimental data based on specific parameters or constants. These equations have been developed by geochemists to describe the kinetics of adsorption

that a particular system follows. The Langmuir and Freundlich models are the isotherms most commonly used to represent the behaviour of adsorbent and adsorbate (free ion) in the field of wastewater treatment. The Langmuir isotherm was presented in 1916 by American chemist Irving Langmuir (Langmuir 1918). This model assumes monolayer coverage of the adsorbate to the adsorbent; all binding sites are equally probable; and that it is a second-order reaction. This model is represented by the following equation:

(1) $$q = q_{max} \frac{K_L C}{1 + K_L C}$$

where q is the amount of solute (i.e. phosphate) adsorbed per unit of solid at equilibrium, q_{max} is the maximum adsorption capacity, c is the equilibrium concentration of solute remaining in solution, and K_L is a constant.

The Freundlich adsorption isotherm, an empirical model, was established in the early twentieth century by German scientist Herbert Freundlich (Freundlich 1906).

(2) $$q = K_F C^{1/n}$$

where K_F is a measure of adsorption capacity, and 1/n is an indication of intensity of adsorption. The higher these values are, the greater the maximum capacity and the more favourable the adsorption.

Because it has two parameters, the empirical Freundlich isotherm often exhibits a better fit for collected adsorption data, especially on non-uniform surfaces (Vuong and Monson 1998). However, because the theoretical Langmuir model has a rational basis, it was the isotherm that was chosen to fit the adsorption data in this study.

1.4 *Microbial oxidation of iron*

Microbial activity is an important part of iron cycling in the biosphere, and is dependent on redox (reduction-oxidation) reactions carried out by certain types of bacteria,

including carbon fixation and adsorption (Fortin & Langley 2005). Iron oxides can also form via oxidation of ferrous iron by iron-oxidizing bacteria, resulting in what are known as biogenic or bacteriogenic iron oxides (BIOS). They are produced in natural environments as a result of metabolic pathways of microorganisms that are able to obtain energy via the removal of electrons from Fe(II) (Emerson and Weiss 2004). This usually occurs at interfaces between oxic and anoxic environments. The mechanism of energy conversion is not well understood, but it is known that the reaction takes place outside of the cell to prevent iron accumulation within (Emerson and de Vet 2015). These types of bacteria must also have a way of transferring the captured electron from the outer cell wall to the cytoplasmic membrane for electron transport, which eventually results in the generation of a molecule of high-energy adenosine triphosphate (ATP) (Emerson 2012).

A key characteristic of many iron-oxidizing bacteria such as species from the *Gallionella* and *Leptothrix* genera (neutrophiles) is the formation of an exopolysaccharide sheath surrounding each organism. Once these bacteria oxidize iron as a source of metabolic energy, they excrete a gel-like biopolymer in which iron oxides are contained. This structure is vital to the bacterium because it prevents the build-up of iron oxides within the organism, which could result in encrustation (Chan et al. 2009), and the formation of a hard coating around the cell that may result in death. The presence of this is extracellular polysaccharide matrix is one of the main reasons why the iron oxides within them have such a high adsorptive capacity. Their application to water treatment is effective because of the increased surface area of iron oxides that this exopolysaccharide sheath imparts (Fortin and Langley 2009).

Oxidation reactions by iron oxidizing bacteria can occur in both freshwater and marine settings, including aquifers, soil, sediments, lakes, wetlands, deep-ocean vents, and also in human-engineered infrastructure such as tailings ponds from mine waste (Fortin & Langley 2005). Furthermore, some investigations of these microbes in aquatic environments have observed iron-rich minerals present inside bacterial cells (Bazylinski et al. 1993). Iron oxides can take the form of ordered minerals including goethite, hematite, and magnetite, but commonly as amorphous minerals such as ferrihydrite and green rust (Fortin and Châtellier 2003). Ferrihydrite can be

precipitated straight from an iron-rich solution as well as formed by bacteria as a byproduct of microbial metabolic pathways (Fortin and Langley 2005, and references therein), and its synthesis in a laboratory setting is straightforward.

There are two processes by which iron in solution can be oxidized, and the processes compete for available aqueous iron. In the first, homogeneous oxidation, iron ions are directly oxidized by dissolved oxygen in the water (Lerk 1965). In the second process, heterogeneous oxidation, Fe^{2+} ions are first adsorbed onto an iron oxide surface in order to be oxidized. In this case, the speed of the oxidation reaction is dependent on the amount of iron oxide present (Tamura et al., 1976). The activity of the surface in the heterogeneous process depends on the conditions under which the surface was formed and the composition of the water, including its pH level (Stumm 1993).

Levels of dissolved oxygen have been investigated in water bodies that comprise the habitat of iron oxidizing bacteria. It has been found that these bacteria reproduce best between dissolved oxygen concentrations in the range of 5 to 10 μM (Duckworth et al. 2008) but can live in environments with dissolved O_2 concentrations of up to 100 μM (Bruun et al. 2010). These are considered sub-oxic (low oxygen) conditions. Other studies have shown that iron-oxidizing bacteria are capable of oxidizing iron within a pH range of 6 to 8 (Mouchet et al. 1985). This is a fairly broad range of possible iron-oxidizing activity, however at the higher end of this range, the authors of this study found that dissolved oxygen concentrations must be kept very low in order to maintain the oxidation-reduction potential at a state that allowed heterogeneous iron oxidation (on a surface) to out-compete homogeneous iron oxidation in solution.

1.5 *Microbial reduction of iron oxides*

Iron cycling in terrestrial and aquatic environments occurs as a result of both abiotic and biotic processes. In the absence of oxygen, some types of microbes carry out microbial anaerobic respiration (Lovely 2000), which results in dissimilatory metal reduction. This is a biogeochemical process by which microbes create electrochemical gradients by oxidizing organic matter as the electron donor (such as lactate) and reducing a metal, which acts as the terminal electron acceptor. This mechanism

generates chemical energy necessary for function and growth (Akob et al. 2008). The reduction of ferric iron occurs most often in soils and sediments (Coker et. al 2012). Dissimilatory metal reduction by iron reducing bacteria promotes the formation of secondary minerals (Hansel et al. 2003).

The chemistry of the environment in which iron reduction by microbes occurs is dictated by conditions such as iron concentration, pH, redox potential, and advective flow (Zachara et al. 2002). The secondary mineralization from the reduction of ferrihydrite transpires by coupled biotic and abiotic pathways that produce new minerals, mainly goethite, magnetite, and green rust, and is driven by reaction between the newly reduced ferrous iron and the surface of the remaining ferrihydrite (Hansel 2003). Other minerals can form depending on the presence of nutrients such as phosphate, sulfur, and carbonate. The inclusion of organic matter within the system may also affect mineral formation, inhibiting some and promoting others, as well as the rate of iron reduction and respiration in soils and sediments (Shimizu et al. 2013).

The biochemical pathways undertaken by iron-reducing bacteria are still not fully understood. *Shewanella putrefaciens* has been one of the most-studied microorganisms in this category (along with *Geobacter metallireducens*) and it is known to have an elaborate electron transport system, and is able to use many different elements or molecules as an electron acceptor, including oxygen (Myers and Myers 2000). This bacterium is believed to produce a menaquinone-like molecule that has active redox capabilities, and it has been suggested that it plays a key role in transmitting electrons to ferrihydrite (Newman and Kolter 2000). This may appear to be a risky approach, with high potential for degradation of the carrier molecule by another organism once released extracellularly. However, in the context of surface environments (such as biofilms), expelling a few of these may be cost-effective and favourable for neighbouring cells in the colony (Straub et al. 2001).

Reductive dissolution of iron oxides causes ferrous ions, hydroxide ions, adsorbed species, and co-precipitated compounds to be released back into solution (Roden et al. 2004). However, these components are then likely to form secondary iron oxide minerals (Glasauer et al. 2003) that contain Fe, such as magnetite, goethite, lepidocrocite, and

green rust. Furthermore, depending on the ions present in the environment, previously adsorbed species (prior to reductive dissolution) may too be incorporated into the crystal structure of the mineral, trapping them in a relatively stable configuration. For example, siderite is a ferrous iron oxide mineral that contains carbonate, and vivianite similarly contains phosphate (Hansel et al. 2003). There are many potential influences that control the particular pathway of biomineralization, such as pH, presence and concentration of other ions/compounds, redox potential, advective flow, and most importantly, the availability of Fe(II) (Zachara et al. 2002).

1.6 *Remediation approaches*

There are techniques to remove excess nutrients from a polluted environment. Remediation technologies often make use of organisms to capture pollutants. Nutrient bioextraction generally involves the farming of seaweed or shellfish such as mussels that consume phosphorus and nitrogen, which are incorporated into the organisms' biomass (Emerson and de Vet 2015). Biostimulation is the process of manipulating chemical conditions at a polluted site to promote growth of existing bacteria that are able to remediate certain contaminants via normal cellular processes. Biofiltration comprises several methods of pollution control to sequester and degrade environmental pollutants, and includes constructed wetlands, treatment ponds, and riparian zones. These engineered sites are designed with specific organisms and soils that bind pollutants and excess nutrients (Bashan and deBashan 2004). Inorganic phosphate in particular can be precipitated by metals found in wetland soils, including calcium, aluminum, and ferric iron.

As early as the late 1800s, iron oxidizing bacteria had been thought of by the water treatment industry as troublesome because they caused clogging of pipes and drains, were known to be corrosive, and could cause biofouling (Emerson and De Vet 2015), which is the accumulation of plants, animals, algae, or microorganisms on underwater surfaces (Yebra and Johansen 2004). Ironically, starting in the 1970s, studies have shown that this group of bacteria is important in biofiltration processes (Czekalla et al. 1985). There is great potential for the use of these ubiquitous and naturally occurring bacteria to tackle environmental problems.

Iron oxides have been shown to have the ability to sequester certain toxic contaminants from a variety of environments. Pollutants that can be captured via iron oxides include, but are not limited to: selenium (Chubar et al. 2014), arsenic and nitrate (Li et al. 2015), strontium-90 (Langley et al. 2009), lead (Ma et al. 1993), and phosphate (O'Loughlin et al. 2000). These pollutants are released into the environment from industrial activities such as agriculture, mining, and nuclear plants. When the contaminants are in proximity to soil minerals such as iron oxides, their bioavailability can be reduced (O'Loughlin et al. 2000) through adsorption, which is defined as the bonding of molecules or ions to a substance of another phase (Sancey et al. 2011). This can stabilize the pollutant and prevent it from bioaccumulating in organisms within the ecosystem (O'Loughlin et al. 2000), and/or cause it to be precipitated out of solution.

There has been a significant amount of research conducted in regards to the removal of arsenic from polluted sites via adsorption onto iron minerals (Dixit and Hering 2003). The similar structure and charge of arsenate to phosphate could have implications with respect to methods of arsenic removal being used for phosphate removal. Because they are analogous, some findings of the behaviour of arsenate during pollution remediation may be useful in assessing whether phosphate removal via similar methods is practical.

The application of biogenic iron oxides for removal of phosphorus has been studied to a limited extent (Rentz et al. 2009). Adsorption kinetics and thermodynamics of this process were determined based on samples of biogenic iron oxides and associated bacteria taken from a natural wetland in Idaho, USA. This study concluded that iron oxides produced by iron oxidizing bacteria exhibited excellent adsorption capacity of phosphorus, and offer a potential solution for the persistent problem of nutrient pollution (Rentz et al. 2009). This investigation also discussed the possibility of regenerating the adsorbent, which is an important matter in the practicality for a remediation technique.

In published data on adsorption experiments using biogenic iron oxides, the extent to which an ion will be adsorbed to the surface depends on the availability of complexation sites (Kulczycki et al. 2005). These charged sites can become protonated and

deprotonated, so the pH of the system heavily influences the degree of adsorption that occurs (Langley et al., 2009). The pH range in which an ion adheres to an adsorbent is referred to as the adsorption edge (Guibauld et al. 2006). Since adsorption onto biogenic iron oxide surfaces occurs primarily by inner sphere complexation, phosphate adsorption is highly dependent on the pH and ionic strength of the aquatic environment. However, there is potential for desorption of phosphate back into solution following a decrease in pH or increase in ionic strength. Additionally, desorption can occur when biogenic iron oxides are exposed to microbes capable of anaerobic reduction, which would result in dissolution of the iron, releasing the adsorbed contaminants back into the flow system (Langley et al. 2009).

The study by Rentz and colleagues in 2009 that determined the thermodynamic and kinetic properties of phosphate adsorption to biogenic iron also suggested a method by which biogenic iron oxides could be regenerated during industrial water treatment processes. The authors describe an aggregate filter containing biogenic iron oxides, with water high in aqueous phosphate flowing through. A periodic backwash of the filter would "recharge" the phosphate adsorptive capacity with the removal of spent bacteria that have adsorbed maximum phosphate on the surface of their exopolysaccharide sheaths. Iron-oxidizing bacteria would continue to grow with the addition of more aqueous iron, and the process of filtration-adsorption could be repeated (Rentz et al. 2009). It is practical and cost effective to harness the biofiltration and nutrient control power of naturally occurring iron-oxidizing bacteria, considering their abundance in a variety of aquatic ecosystems. Using microorganisms to remediate a system is a sustainable endeavour, and the use of a single species to do so is economically attractive.

Restricting nutrients such as nitrogen and phosphorus in an aquatic environment is an effective way to mitigate environmental damage. If conducted diligently, limitation of nutrients offers a practical alternative for the prevention of bacteria overgrowth by the treatment of water (Emerson and De Vet 2015). Since microorganisms need phosphate to reproduce and to carry out metabolic processes, limiting its availability in the body of water can prevent biofouling (Vrouwenvelder et al. 2010). Thus, removing excess phosphate from an aquatic system has the potential to prevent both uncontrolled

autotrophic cell growth (i.e. bacterial contamination, eutrophication, algal blooms) and heterotrophic cell growth (animals, fungi, other bacteria) (de Vet et al. 2012 and Lehtola et al. 2002). Both of these possible outcomes could result in disruption of the delicate balance of the food web and ecosystem, and therefore preventative measures of phosphate control should be valued in comparison to remediation after damage has already occurred.

Due to their significant surface area/porosity and positive surface charge (Canecka et al. 2015), biogenic iron oxides yield a suite of useful applications in the field of water treatment. Because of widespread natural occurrence, their use in remediation is inexpensive and practical. Their reactive surfaces have high adsorptive capacity for excess nutrients, arsenic, heavy metals, and radionuclides (Seder-Colomina et al. 2014). The control of nutrients such as phosphate can prevent unwanted bacterial growth, and their removal via harmless and naturally occurring iron oxides presents a safe and economical alternative to the use of strong disinfecting chemicals, which can produce harmful side effects (Emerson and de Vet 2015). The continued research of adsorption of excess nutrients has the potential to be applied to many environmental concerns. In this context, the determination of optimal conditions under which maximum phosphate adsorption of biogenic iron oxides is an appropriate avenue of further research.

This project investigates the chemical conditions at which the iron oxide ferrihydrite has the highest adsorptive capacity for phosphate. Phosphate concentration, pH, and organic carbon content of iron oxides are examined. In nature, there are numerous other variables that can influence phosphate adsorption and retention. In particular, microbial activity, namely microbial iron reduction, can lead to the release into solution of contaminants previously adsorbed onto iron oxides (Fortin and Langley 2005). Therefore, the other research inquiry of this study is an analysis of the behaviour of ferrihydrite and phosphate in the presence of iron reducing bacteria under anaerobic conditions. Both parts will compare the processes in the presence and absence of organic matter. Further exploration and an improved understanding of iron-phosphate interactions and the role of iron reducing bacteria could contribute to the development of more efficient processes by which iron and microbes can be used for technology within the fields of industrial water treatment and environmental remediation.

2. Methodology

2.1 *Ferrihydrite and co-precipitate synthesis*

Most adsorption and all reduction experiments were conducted using the amorphous ferric mineral ferrihydrite ($Fe^{3+}_2O_3 \cdot 0.5H_2O$) due to its prevalence in aquatic systems, its ease of preparation in the laboratory, and its ability to be co-precipitated with varying amounts of organic matter. The polysaccharide alginate ($C_6H_8O_6$) was used as the organic matter component of synthetic co-precipitates.

The protocol for ferrihydrite synthesis was derived from the methods of Mikutta et al. (2008). Ferric chloride ($FeCl_3$) was first dissolved into deionized water in a large beaker on a magnetic stir plate with a pH probe inserted. A burette filled with 1 M sodium hydroxide (NaOH) was set up, and the base was first rapidly and then slowly added to the stirring solution, until reaching pH 7. This resulted in the hydrolysis of Fe(III) and the subsequent precipitation of ferrihydrite).

For the synthesis of alginate-ferrihydrite co-precipitates, alginate was first left to dissolve in 500 mL of deionized water overnight. Ferric chloride was dissolved in 50 mL of water and added to the alginate solution after adjusting the pH of the alginate to 2.5 with 1 M hydrochloric acid (HCl) in order to prevent the immediate precipitation when combining, which would affect the homogeneity of the mineral. Sodium hydroxide (NaOH) was added to the alginate-iron solution in the same manner as previously described. The resulting amorphous mineral was allowed to settle in the beaker before removing the excess of saline solution and pouring contents into 50 mL falcon tubes. The samples were then centrifuged for 8 minutes at 3100 rpm, the supernatant was removed, and fresh deionized water was added. Each tube was vortexed to re-suspend the pellet. This rinsing process was carried out 4-5 times. Synthetic samples were stored in the falcon tubes at 4°C for up to 2 weeks for pure ferrihydrite, and up to 2 months for the co-precipitates.

2.2 *Physico-chemical characteristics of the co-precipitates*

2.2.1 *Water and organic content*

Water and organic contents were determined for select samples used in the adsorption experiments. The measurements were carried out with foil weigh boats, which were pre-weighed. An amount of sample was placed into each weigh boat, masses were recorded, and samples were left to dry in an oven for 24 h at 100°C. Masses were recorded again. The ratios of the original and final masses were used to calculate the water content. Samples were then placed in an oven for at least 16 h at 375°C. Loss on ignition (LOI) allows for the determination of organic carbon content. The difference in mass after removing the sample from the oven and letting it cool in a desiccator was used to calculate the percentage of organic carbon.

2.2.2 *TIC TOC analysis*

Select samples were analyzed at the University of Ottawa's G.G. Hatch Stable Isotope Laboratory to quantify the organic carbon content of the samples using the Elementar vario ISOTOPE cube. Dehydrated co-precipitates that had not gone through loss on ignition were ground into a fine powder using a mortar and pestle. Approximately 0.02 g of sample was weighed very accurately into a small foil canister. The foil was then carefully formed into a tiny round ball with tweezers. The samples were then handed over to the laboratory operators to run through the instrument, which has a detection limit of 0.1% C.

2.2.3 *Iron content determination*

The iron content (obtained from acid digestion, see section 2.4.5) was determined with the Ferrozine colorimetric assay, according to the method of Stookey (1970). Approximately 0.01 g of wet sample was weighed into a vial and the exact weight was recorded. Hydrochloric acid (HCl) and oxalic acid ($C_2H_2O_4$) were added (10 mL each) to each vial along with a small stir bar inside, and the sample was left to dissolve on a magnetic stir plate for 1 hour. For total iron analysis, 0.1 mL of the digested sample was then added to 0.9 mL of a hydroxylamine (H_3NO) and HEPES buffer (4-(2-

hydroxyethyl)-1-piperazineethanesulfonic acid) into a microfuge tube to ensure that all ferric chloride in the solution was reduced to ferrous chloride. This was left for approximately 20 minutes before carrying out the analysis. 0.9 mL of 2 mM ferrozine solution (sodium 4-[3-pyridin-2-yl-5-(4-sulfophenyl)-1,2,4-triazin-6-yl]-benzenesulfonate) was pipetted into plastic cuvettes, along with 0.1 mL of each digested and reduced sample. The HACH spectrophotometer was set to a wavelength of 562 nm and the instrument was zeroed with a plain ferrozine solution. Using a pre-constructed standard ferrozine curve (see Appendix, Figure A1), the iron content of the samples was determined.

2.2.4 *Surface charge of iron oxides*

Acid-base titrations were carried out to determine the approximate point of zero charge, which is the pH condition at which the net surface charge of the sample is zero. About 1 g of wet co-precipitate sample (1.0 g alginate/L ferrihydrite suspension) was dispersed into a large beaker containing 500 mL of 0.001 M sodium nitrate ($NaNO_3$) using a magnetic stir bar and plate. The suspension was bubbled with nitrogen for 20 min to remove any dissolved carbon dioxide. To ensure that the nitrogen going into the beaker contained no carbon dioxide, it was pre-bubbled or scrubbed through an apparatus of 2 Erlenmeyer flasks, one containing a weak base and another containing deionized water. A calibrated pH probe was inserted into the suspension and 3 mL of 0.01 M nitric acid (HNO_3) was added to bring the pH down to 4.25, the starting point of the titration. 0.5 mL of 0.01 M sodium hydroxide (NaOH) was then added every 3 min, with the change in pH recorded each time until pH 9 was reached. The process was then reversed: 0.5 mL of 0.01 M of nitric acid was added at intervals of 3 minutes, with pH change recorded each time, until the pH came back down to 4.

The zeta potential is a measurement of the electrical charge near the diffuse layer around a particle in a colloidal dispersion (Kosmulski 2002). Zeta potential measurements of iron-alginate co-precipitates were taken using a Malvern Zetasizer Nano instrument, at the Centre for Catalysis Research and Innovation, Department of Chemistry and Biomolecular Sciences, University of Ottawa. A concentration of 1 g of wet mass per litre of electrolyte solution was chosen. Sodium chloride (0.01 M NaCl)

solution was used as the electrolyte, which was first passed through a 0.2 nm filter to ensure all dust particles were removed. Dust can affect the instrument measurements so contamination should be avoided. For each sample, suspensions were adjusted to pH 5, 6, 7, 8, and 9, using filtered solutions of 0.001M NaOH or 0.001M HCl. Approximately 1.5 mL of each sample was syringed into a capillary cell and quickly inserted into the Zetasizer Nano to begin the measurements. This was done in triplicate. It is time-sensitive because the colloidal dispersion will settle over time, and measurements are best taken in a uniform dispersion. Between each sample, the capillary cell was rinsed 3 times with electrolyte with a 1 mL syringe. Zeta potential measurements were taken across a range of pH in order to confirm the point of zero charge, so this value could be compared across samples.

2.3 *Adsorption experiments*

Kinetic experiments were first performed in order to determine the time it takes for phosphate to fully sorb onto the surface of the iron mineral particles. 0.05 g of wet ferrihydrite and/or co-precipitate was weighed and added to 15-mL falcon tubes and the exact mass recorded. 9.95 mL 0.01 M sodium chloride was added to each tube (14 in total), which were then vortexed. 30 μL of 1000 ppm phosphate stock solution (made by dissolving 1.43 g KH_2PO_4 into 1 L deionized water) was added to each tube for a final concentration of 3 ppm. An additional kinetic experiment was conducted using a starting concentration of 9 ppm. Each of the 14 tubes was placed on a rotating shaker instrument. At different time intervals, tubes were removed in duplicate and sub-samples were taken with a syringe and filtered with a 0. 2 μm filter. The initial kinetic experiment used the following time intervals: 5 min, 15 min, 30 min, 1 h, 2 h, 24 h, and 48 h. Once it was determined that adsorption was still occurring at the 48 h mark, another kinetic experiment was conducted that used the time intervals of 10 min, 1 h, 8 h, 24 h, 48 h, 72 h, and 96 h. The concentration of phosphate in the filtered fraction was determined with the molybdenum blue method (see section 2.3.1). When concentrations are graphed, phosphate remaining in solution should decrease over time as adsorption to iron occurs and then level off. The start of the plateau indicates the time at which adsorption has gone to completion (See appendix, Figure A3).

Adsorption experiments were conducted with co-precipitates of varying content of organic carbon, pure ferrihydrite (zero organics) and natural samples of biogenic iron oxides that were collected from the New Calumet mine in Québec, Canada. A small amount of sample was weighed out (depending on iron content, to result in a concentration of 300 μM Fe) (see Table 1) and suspended into a sodium chloride solution (0.01 M NaCl). Phosphate (from the stock solution) was added to yield initial concentrations of 0, 3, 6, 9, 12, 15, and 20 ppm. The suspensions were adjusted to pH 7 and left on the rotary shaker for 48 h. This time interval was chosen as a standard for all subsequent adsorption experiments. Even though it had been determined during the preliminary kinetic experiments that some adsorption continues to occur after 48 h, the vast majority occurs within the first 2 days. At this point, samples were either filtered or centrifuged, and supernatant/filtrate was then analyzed for its phosphate content using the molybdenum blue method.

pH-dependent adsorption experiments were also performed in order to determine the influence of pH on the degree of phosphate adsorption onto iron oxides. The samples (equivalent to 300 μM Fe) were suspended in 10 mL of NaCl (0.01 M) in 15-mL falcon tubes. The initial concentration of phosphate was set to 9 ppm for all samples. Before leaving the samples to equilibrate on the rotary shaker for 48 h, the pH was set, in duplicate, to 4, 5, 6, 7, 8, 9, and 10 using HCl and NaOH. Samples were then centrifuged at 3100 rpm for 8 minutes, and the supernatant was analyzed for its phosphate content.

2.3.1 *Phosphate measurements*

The molybdenum blue method (Johnson and Pilson 1972, Dhar 2004) was used to determine the aqueous (filtered fraction) phosphate concentrations. The solution was prepared as follows: 0.22 g ascorbic acid ($C_6H_8O_6$) was weighed into a vial with a small stir bar and dissolved in 2.00 mL water for about 5 minutes on a magnetic stir plate. 2.00 mL of 24 mM ammonium molybdate ($(NH_4)_6Mo_7O_{24}$) was added which caused the solution to turn bright yellow. After a few minutes, 1.00 mL of 8 mM potassium antimonyl-tartrate ($C_8H_{10}K_2O_{15}Sb_2$) was added. Within a few minutes, the solution turned an indigo blue colour. Finally, 5.00 mL of 2.5 M sulfuric acid (H_2SO_4) was added.

The solution was always freshly prepared on the day it was used due to the relatively quick degradation of the ascorbic acid.

For the sample analysis, 4.4 mL of 0.12 M (1%) hydrochloric acid (HCl) was added to each of a set of empty scintillation vials, and 0.4 mL of each sample (the supernatant or filtrate) was added to its respective vial. Then 0.4 mL of freshly prepared molybdenum blue colour reagent was pipetted into each vial. After 1 hour, about 1.6 mL of each sample was poured into a new cuvette and inserted into a HACH spectrophotometer. The absorbance was read at a wavelength of 880 nm. Absorbance values are then inputted into a previously constructed calibration curve that was made with standards of known phosphate concentration (See appendix Figure A2).

2.4 *Bacterial reduction with* Shewanella putrefaciens *CN32*

Two sets of bacterial reductions were carried out under anaerobic and sterile conditions over a period of 15-20 days each. For the first one, pure ferrihydrite was used, and for the second, a co-precipitate of 1 g alginate/L was used. In the following paragraphs, 'iron oxides' will be used to describe either pure ferrihydrite or co-precipitate. Each reduction experiment consisted of 5 treatments inside 1 L Pyrex bottles: a control containing iron oxide but no bacteria; iron oxide and bacteria in duplicate; and iron oxide with pre-adsorbed phosphate and bacteria, also in duplicate.

2.4.1 *Pre-adsorption of phosphate to iron oxides*

One of the primary goals of these reduction experiments was to examine the behavior of phosphate adsorbed to the surface of iron oxides when bacterial reduction occurs. For this reason, two treatments in each reduction experiment contained iron oxides that had been fully covered in negative phosphate ions. To do this, first a digestion was carried out on the fresh batch of iron oxides to determine the exact iron content. Approximately 3 times the amount of wet mass needed for 1 microcosm (to result in an iron concentration of 4 mM) was measured out into a 1 L Pyrex bottle with 800 mL sterile 0.01 M sodium chloride solution. 2.2 mL sterile 1 M phosphate solution was added to the bottle and cap was well tightened. This was placed on the shaker bath for

48 h at 150 rpm. Based on kinetic experiments, it was assumed that the majority of the phosphate adsorption occurred within this time period. The solids were removed from the shaker and left to settle. The excess water was removed and the remaining solids were centrifuged and washed once to remove excess phosphate. An acid digestion was carried out on this portion of iron oxide material to check the iron content, which may have changed during the phosphate adsorption and washing steps.

2.4.2 *Culturing* Shewanella putrefaciens *CN32*

Shewanella putrefaciens CN32 was pre-cultured on agar plates prior to be cultured in a liquid medium (sterile tryptic soy broth (TSB)) on a shaker bath at 160 rpm for 24 h. The culture was then transferred to a mixture of 25 mL TSB and 25 mL of chemically defined medium (CDM) (see composition outlined in Appendix, Table A1) to obtain a ratio of 50:50. After 24 hours, the culture was transferred into of series of TSB/CDM mixtures having ratios of 95:5, 99:1, and finally 100% CDM. 100 mL CDM was then added to glass bottles along with 4 mL of the bacterial culture grown in 100% CDM and 39 μL of the 1 M phosphate stock solution for a finale PO_4 concentration of 390 μM. These flasks were left to grow on the shaker bath for 36 hours at 200 rpm. On the day of inoculation, the ~400 mL of culture in 100% CDM were transferred into 9 or 10 50-mL falcon tubes and centrifuged at 3000 rpm for 10 minutes. The supernatant was poured off and 30 mL fresh sterile CDM was added to the tubes, which were vortexed to re-suspended. The tubes were centrifuged again, the supernatant poured off, and 2 mL of CDM was added to each tube, which were vortexed and combined into 1 falcon tube of inoculum.

2.4.3 *Set-up and inoculation*

A known amount of iron oxides (equivalent to a final iron concentration of 4 mM of Fe) was added to 700 mL of sterile CDM in Pyrex bottles, along with sterile phosphate solution (for a final concentration of 390 μM). The amount of inoculum was determined with the Bio-rad protein assay. The inoculum was pipetted into each microcosm. No bacteria were added to the control.

2.4.4 *Sampling procedure*

On the day of inoculation (t=0), and at subsequent intervals of approximately 48 hours, sub-samples were taken from the bottles to monitor changes in ferrous iron, bacteria, phosphate, pH, and redox potential. The following steps were carried out for each microcosm. The Pyrex bottle was shaken vigorously and the cap was removed. A sterile 20-mL scintillation vial (subsample vial) was filled with the contents of the microcosm. From this vial, about half was poured into a 10-mL syringe with a 0.2 nm filter and filtered into another sterile vial. 0.5 mL of sample was taken from each of these 2 vials and pipetted into 15-mL falcon tubes containing 4.5 mL of 0.5 M hydrochloric acid. These were later used for ferrous iron analysis via the ferrozine method. 5 mL from each of the two sterile vials (one unfiltered, one filtered) were pipetted into 2 new/acid-washed vials, which would later be used for an acid-peroxide digest to analyze for phosphate and total iron. 0.5 mL was taken from the subsampling vial (containing unfiltered sample) and pipetted into a microfuge tube for bacterial quantification. Before each removal of fluid from the subsample vial, the contents were swirled to suspend sediments as evenly as possible. A redox probe (Corning redox Platinum and Ag/AgCl combination electrode) was inserted into the subsample vial (still within the anaerobic chamber) to measure the redox potential (Eh). The pH of the subsample vials was measured with a Mettler-Toledo InLab probe attached to a VWR Scientific pH meter. In a sterile setting, a serial dilution was carried out on each of the microfuge tubes containing 0.5 mL of sample from each microcosm except for the control, using sterile CDM as the diluent. 0.1 mL from the two dilutions of 10^{-4} and 10^{-5} for each sample were spread onto agar plates, as well as 0.1 mL from the undiluted control. These were left to grow for about 48 hours. The colonies that had grown on each plate were then counted and recorded.

Since sampling occurred every two days, the ferrous iron analysis of the 0.5 M hydrochloric acid digests (15-mL falcon tubes) was carried out on the day in between using the ferrozine method. The ferrous iron concentrations determined from this analysis increased over time as the ferric iron from the iron oxides was reduced to ferrous iron by *S. putrefaciens*. Once a plateau in ferrous iron concentrations was identified, it was concluded that the reduction had gone to completion within the given

conditions. At this point, the microcosms were left to allow the sediments to settle. Within the anaerobic chamber, the excess water was removed and the wet sediments were poured into 50-mL falcon tubes. These were removed from the chamber, centrifuged, and then brought back into chamber. The supernatant was poured off and deoxygenated water was added. This washing process was carried out 4 times. The sediments from each microcosm were poured into large plastic weigh boats and left to dry within the anaerobic chamber.

2.4.5 *Sample digestion*

In the fume hood, 1.67 mL of trace metal grade concentrated nitric acid and 3.33 mL of hydrogen peroxide was added to each of the vials containing exactly 5 mL of either unfiltered or filtered sample. Caps were loosely replaced and the vials were placed in an oven at 70°C for 24 h. The vials were then removed, left to cool for 2 h, and then capped again. Once total iron and soluble phosphate analyses were carried out using the colorimetric methods, select samples from the digestion were analyzed using Inductively Coupled Plasma Mass Spectrometry (ICP-MS) to verify total iron and phosphate measurements. The digested samples were prepared for ICP-MS analysis by diluting 1 mL of sample with 9 mL of trace metal grade 1% nitric acid (HNO_3), and then analyzed with an Agilent Technologies 8800 ICP-MS Triple Quad instrument in the Geochemistry Laboratory within the Department of Environmental and Earth Sciences at the University of Ottawa. Standards of iron and phosphate were first run through the mass spectrometer to create a calibration curve.

2.4.6 *Characterization of the post-reduction precipitates*

2.4.6.1 XRD analysis

Once sediments from the microcosms were left for several days to dry in the anaerobic chamber, they were ground into a fine powder inside the anaerobic chamber using a mortar and pestle so they could be analyzed using an X-ray diffraction (XRD) instrument. The mineral powder was carefully loaded onto a sample holder inside the anaerobic chamber. This holder included a dome made of beryllium that was

impermeable to air but would allow X-rays to pass through. The sample holder was placed in an airtight container for transport to the XRD lab. The sample holder was then inserted into a Rigaku Ultima IV diffractometer. The sample is rotated throughout the data collection process for a complete analysis of the crystal structure of the mineral. The instrument parameters were set to take a reading each 0.02 of a degree from from 5° to 80°, an angle known as known as 2θ. Inside the diffractometer, an incident beam and reflected beam form an angle of θ with the crystal plane, and so reflections with respect to the incident beam creates a reflected beam at an angle of 2θ from the incident ray. The peaks that arise at different angles along the 2θ x-axis are unique to each mineral, and the data gathered from an XRD run can be compared to published reference patterns. The peaks were graphed as a scatter plot by a measure of relative intensity (y-axis) and the locations of the prominent peaks were compared to standard mineral patterns to determine presence of specific minerals.

2.4.6.2 SEM analysis

A small amount of each dried and ground mineral sample was observed with a JEOL 6610LV Scanning Electron Microscope (SEM) to help characterize the mineral. Samples were loaded onto a small metal sample holder with a small black double-sided sticker. Sample holders were loaded together into the microscope and viewed with the help of individuals trained on the proper use of SEM. Photographs of each sample at 2 different levels of magnification were captured, at a voltage of 1.7 kV.

3. Results

3.1 *Characterization of Iron Oxides*

Since most experiments were conducted on synthetic iron oxides, iron content measurements (via acid digestion) were carried out on all iron oxides that were either synthesized or collected so that realistic comparisons between natural and synthetic samples could be made. The most important characteristic is iron content, however water and organic content were also measured on select samples to get a sense of the ratios of the components. Table 1 summarizes these characteristics.

Table 1. Characteristics of natural and synthetic BIOS used for adsorption and reduction experiments.

Sample description	Fe content (µmol/g wet)	C content (% dry)	LOI (% OM)	Water (%)
Laboratory synthesized pure ferrihydrite	664	<0.9	ND	ND
Synthetic co-precipitate made with 0.25 g alginate/L $FeCl_3$ solution	517	3.7	21	ND
Synthetic co-precipitate made with 0.5 g alginate/L $FeCl_3$ solution	130	5.6	25	ND
Synthetic co-precipitate made with 0.75 g alginate/L $FeCl_3$ solution	89	8.6	33	ND
Synthetic co-precipitate made with 1.0 g alginate/L $FeCl_3$ solution	57	10	31	98.6
Synthetic co-precipitate made with 2.0 g alginate/L $FeCl_3$ solution	59	13.2	ND	ND
CA-02 - Natural sample, New Calumet mine in Québec, Aug 2015: sampling site on top of a tailings pile with scarce vegetation	2301	ND	14	ND
CA-03 - New Calumet mine Aug/15: sampling site is 4 m downstream of discharge zone of anoxic Fe(II)-rich groundwater	2132	ND	13	ND
CA-04 - New Calumet mine Aug/15: sampling site is at discharge zone of anoxic Fe(II)-rich groundwater	2414	2.7	15	ND

**ND = not determined*

3.1.1 *Water content*

After weighing out approximately 6 grams of wet iron oxide co-precipitate that was made using 1 g alginate/L $FeCl_3$ solution and drying it in an oven at 100-105°C for 24 h, it was determined that the synthetic samples consisted of on average 98.6% water.

3.1.2 *Organic content*

Although a known amount of alginate is added to the system when synthesizing a co-precipitate, the proportion that is actually incorporated into the solid mass cannot be determined based on the input (i.e. some alginate may remain in the liquid phase as the solid mineral forms). After conducting a loss-on-ignition experiment, it was found that roughly 30.5% of the dry mass of a co-precipitate was organic matter: organic carbon, hydrogen, and oxygen. When verifying this organic content by sending samples to the isotope lab for analysis, the result that was returned was a percentage of just carbon. Analysis of carbon content from the G.G. Hatch Isotope Lab yielded an average of 10% carbon for the same batch of co-precipitate. This discrepancy is primarily due to the difference between carbon and organic matter. The chemical formula of alginate is $C_6H_8O_6$, so based on the atomic mass of each of the elemental components and their ratio, a theoretical correction factor of 2.44 accounts for the difference (C mass : total mass). When applied to the total carbon content, a result of approximately 21% organic matter is obtained. The difference can likely be attributed to the loss of structural water within the ferrihydrite ($(Fe^{3+})_2O_3 \cdot 0.5H_2O$) in addition to the carbon and water lost from the alginate.

3.1.3 *Iron content*

Iron content varied between each batch of laboratory-synthesized ferrihydrite and co-precipitate, as well as in the collected field samples that were analyzed. Table 1 includes the iron content of each sample. The primary reason for this determination is to ensure that adsorption experiments can be normalized to a specific amount of iron present, as per the methods of Rentz et al. (2009). In the adsorption results below, the y-axis measures the amount of phosphate adsorbed per unit iron.

3.1.4 *Surface charge of iron oxides*

Zeta potential measurements of several co-precipitates were collected using the Malvern Zetasizer, as laid out in Section 2.2.4. Since the surface charge of a particle is dependent on the concentration of hydrogen ions in solution, Figure 1 shows the zeta

potential as a function of pH for the following co-precipitates: pure ferrihydrite, 3.7% C, and 5.6% C. It was found that the more organic matter that was present in the co-precipitate, the more negative the overall zeta potential measurements were. The pH level at which the zeta potential is 0 mV is known as the point of zero charge of a substance. Figure 1 shows that for ferrihydrite, the function crosses the x-axis at a pH of approximately 7.2, and for the 3.7% C co-precipitate, at pH 6.5. The run conducted for the co-precipitate containing 5.6% C shows that within a pH range of 4 – 8, all measurements taken were well below 0, indicating that the organic matter in the co-precipitate significantly affects the surface chemistry of iron particles in a colloidal dispersion. Since ferric iron dissolves in solution at a pH of around 3.5, zeta potential measurements were not taken below pH 4.

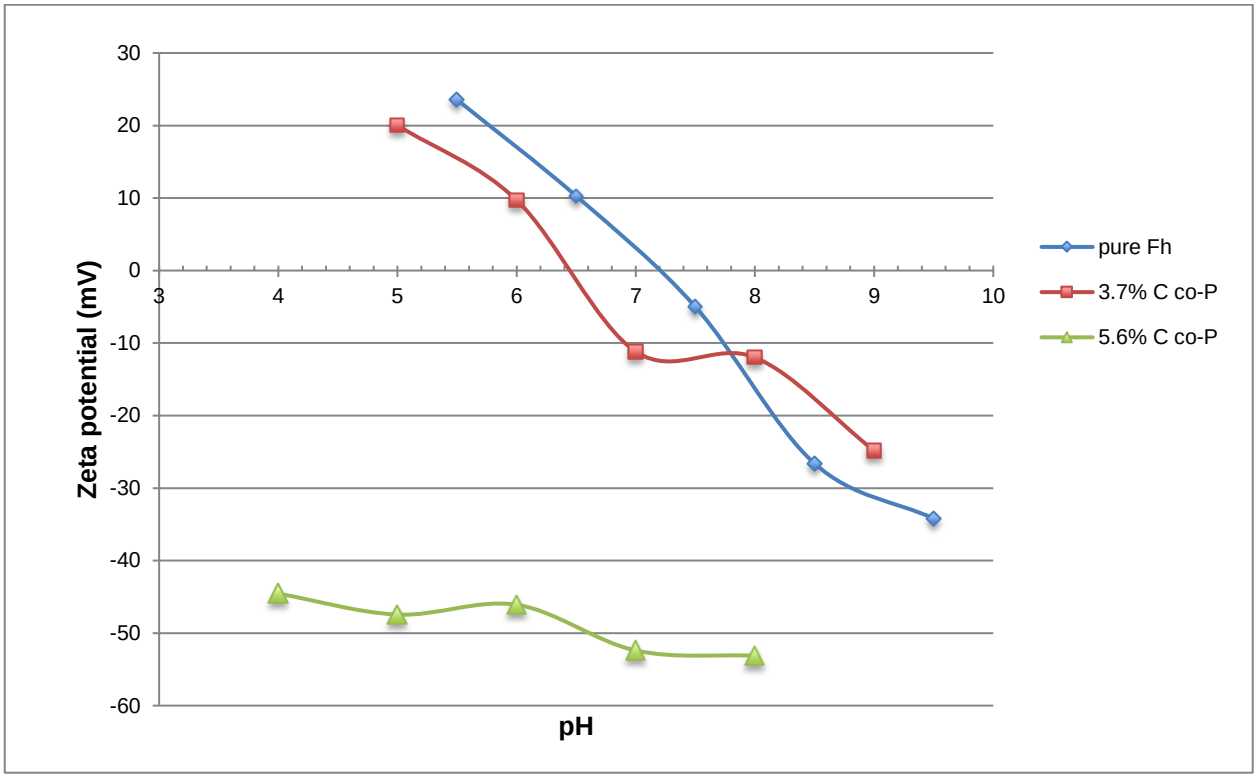

Figure 1. The zeta potential of the surface of ferrihydrite and ferrihydrite-alginate coprecipitate particles as a function of pH. The pH point at which the zeta potential is equal to zero is known as the point of zero charge.

3.2 *Adsorption experiments*

3.2.1 *Phosphate adsorption kinetics*

To maximize efficiency while designing further experiments, a kinetic experiment was first carried out to determine the approximate timeline of phosphate adsorption. It was hypothesized that the vast majority of phosphate adsorption to the surface of iron solids would occur within the first minute of combining. While the majority did adsorb within the first minute, it was found that adsorption continued until several days after the phosphate solution was added to the colloid mixture of iron-alginate co-precipitate. Appendix Figure A2 shows the proportion of adsorption as a function of time for the preliminary kinetic experiment. A co-precipitate containing 1 g/L alginate was used.

3.2.2 *Phosphate adsorption to iron co-precipitates with varying levels of organic matter*

From the kinetic experiment results, a time interval of 48 h was chosen for subsequent sorption experiments. Each run used a sample of differing organic content. Table 1 lists the samples analyzed in this series of experiments shown in Figure 2 (i.e., the amount of phosphate sorption per unit iron for each run using a different co-precipitate as the adsorbent).

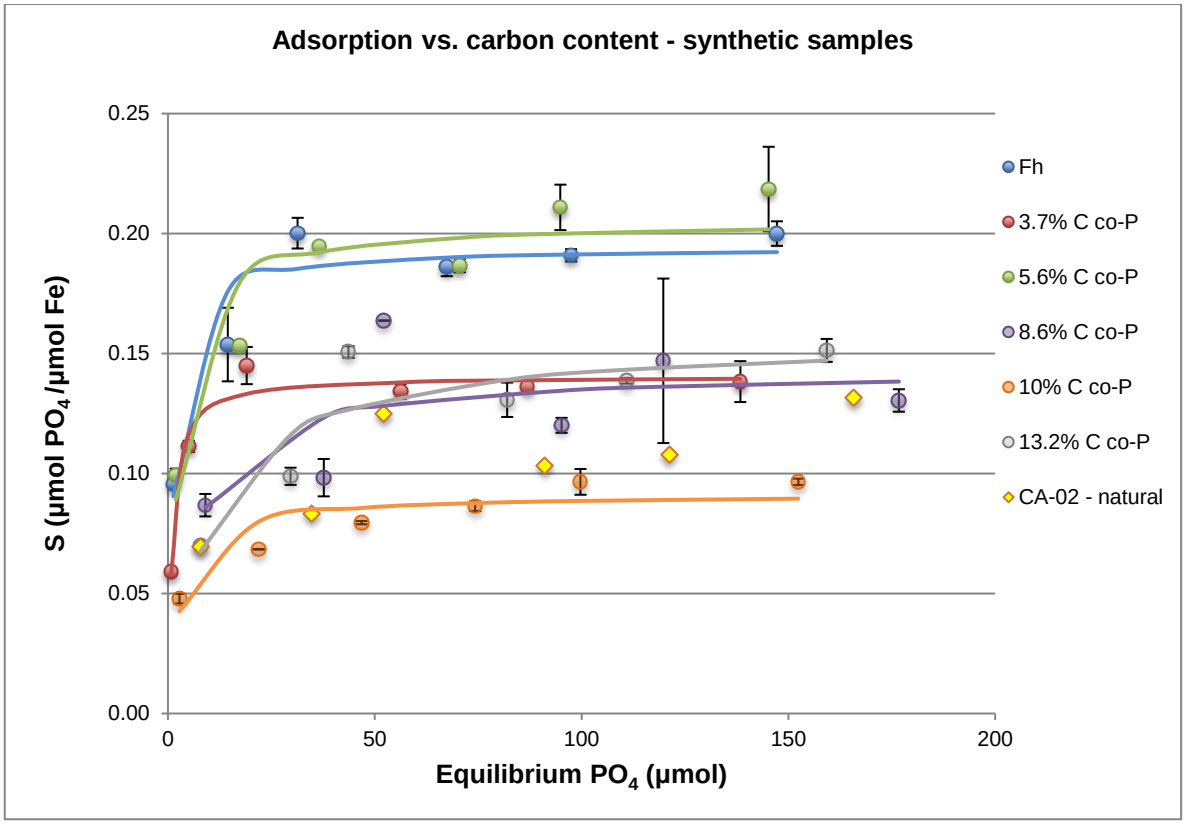

Figure 2. Each set of coloured points represents the equilibrium adsorption experiment that was conducted on each ferrihydrite-alginate co-precipitate that was lab-synthesized. S, the amount of phosphate adsorption per unit iron present in the suspension, is plotted as a function of phosphate concentration remaining in solution at the conclusion of the experiment. The yellow points represent a trial conducted with a natural sample. Trend lines for each data set were created using the Langmuir isotherm.

For comparison, data from the trial of one of the three natural samples was also included in Figure 2. The most efficient adsorbent of the three natural samples fits within the range of efficiency of the synthetic samples. Figure 3 compares the adsorption results for the three natural samples.

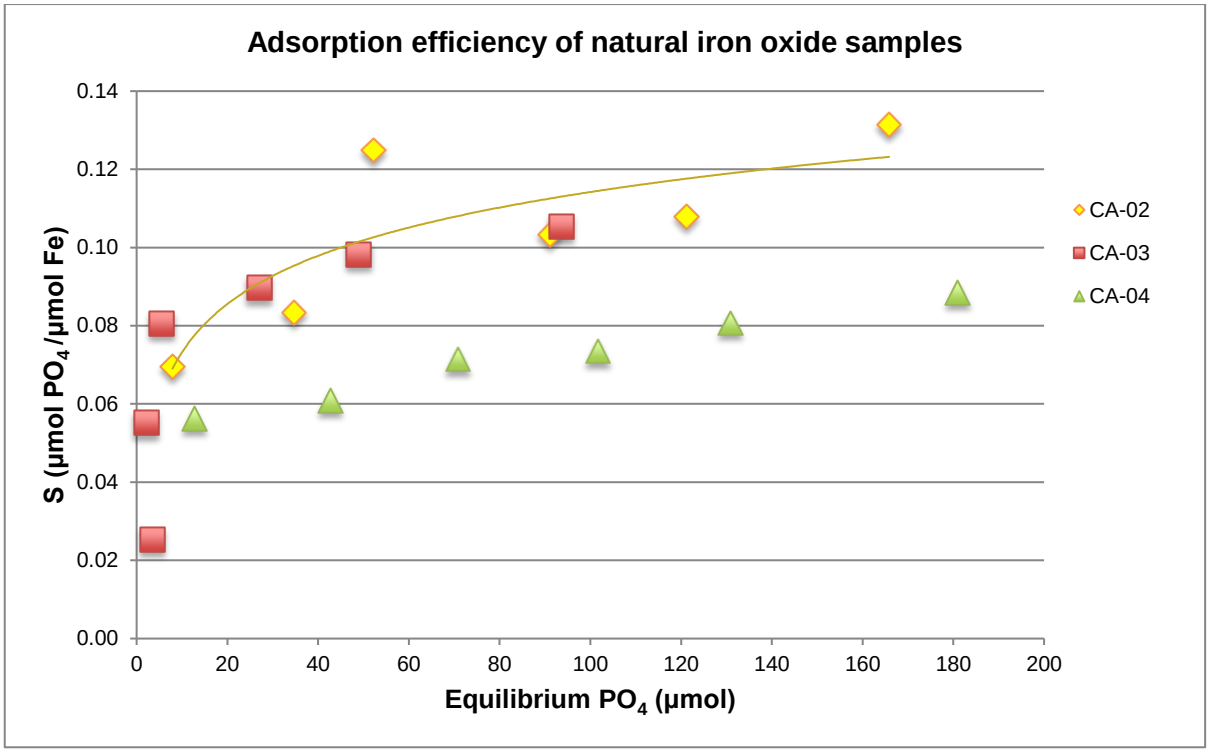

Figure 3. Adsorption of phosphate to natural samples collected from Calumet mine plotted as a function of the equilibrium concentration of phosphate after 48 h. These samples show a similar behaviour and efficiency of synthetic samples.

3.2.3 *pH and adsorption*

Three trials of pH adsorption experiments were conducted. Figure 4 shows that with pure ferrihydrite, 13.2% C co-precipitate, and a natural sample collected from the New Calumet mine, more phosphate adsorbed in systems with a lower pH. This trend was visible regardless of the adsorbent being pure ferrihydrite, a co-precipitate with high organic content, and a natural sample that contained more than just iron minerals and organic matter. Due to the dissolution of iron at around pH 3.5 - 4 (Schwertmann 1991), the pH of these trials was only brought as low as 4.5 or 5.

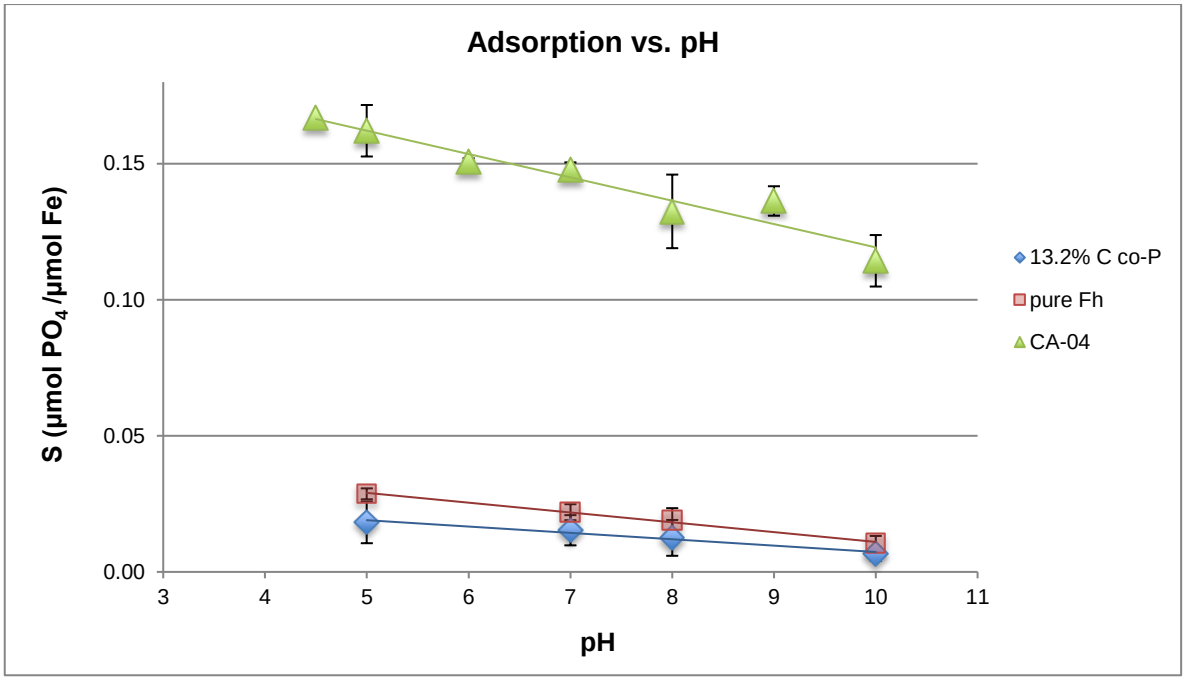

Figure 4. pH linearly influences adsorption of phosphate to iron oxides. As the pH decreases, the amount of adsorption increases.

3.3 *Bacterial reduction experiments*

Two sets of bacterial reductions were carried out with the *S. putrefaciens* CN-32 strain, an iron-reducing microbe. One experiment was carried out with pure ferrihydrite, and the other with a co-precipitate that was made with 1 g alginate/L $FeCl_3$ solution, producing a co-precipitate with relatively high C content (approximately 10%). Within each, two trials were conducted with phosphate pre-adsorbed onto the iron oxide, and two trials were conducted without. There was also a control microcosm that contained no bacteria.

3.3.1 *Rates of reduction*

Figure 5 represents the reduction of Fe(III) to total Fe(II) over time that occurred within the reduction experiment containing pure ferrihydrite. These reductions were conducted over a span of 23 days under anoxic conditions. The maximum rate of reduction tended to occur within the first week after inoculation. When phosphate had not been sorbed to the iron oxide in advance of the reduction, the maximum rate was

1.9% reduction per day, and when phosphate had been pre-sorbed to the iron oxide, the maximum rate of reduction was 7.3%/day. As the control system contained no bacteria and only pure ferrihydrite with CDM, no iron reduction was observed. This indicates that the control microcosm experienced no contamination with iron-reducing bacteria throughout the course of the experiment.

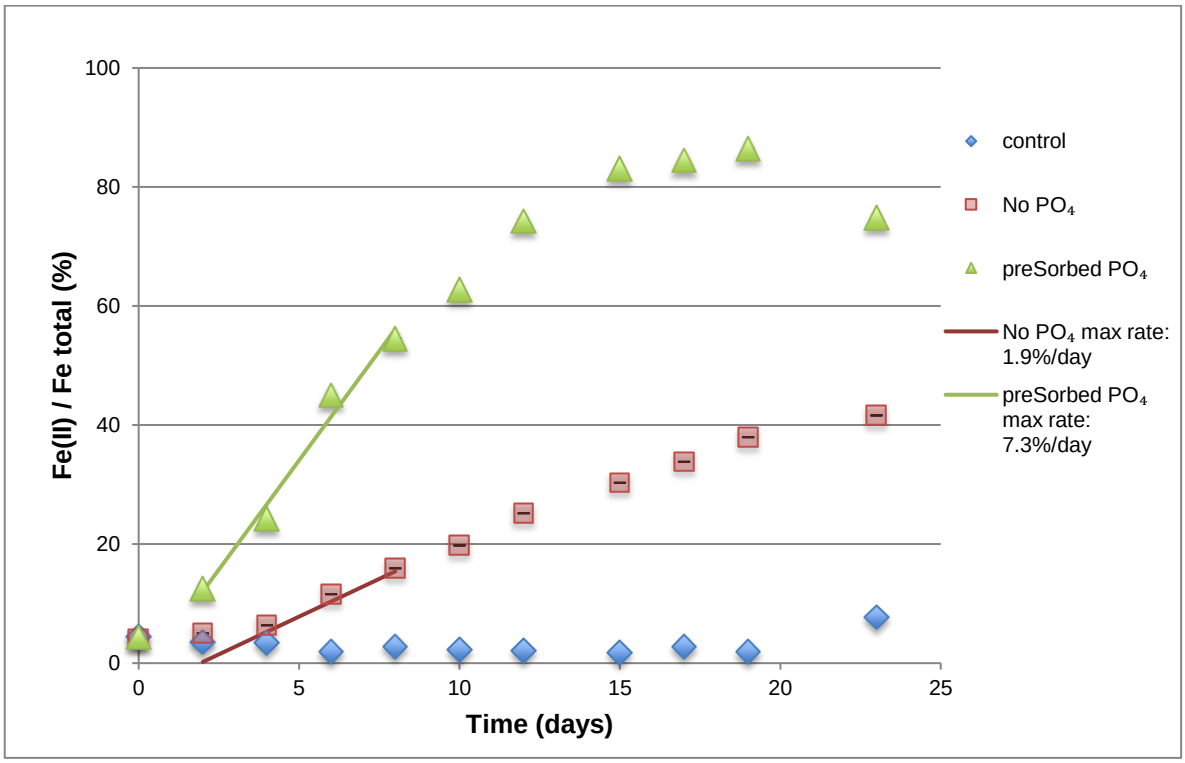

Figure 5. Reduction of Fe(III) to total Fe(II) by *S. putrefaciens* over time. Ferrihydrite with sorbed phosphate was reduced much faster and to a greater degree of completion than ferrihydrite with no sorbed phosphate.

Figure 6 shows the behaviour of the co-precipitate containing 10% C over time when exposed to iron reducing bacteria under anaerobic conditions.

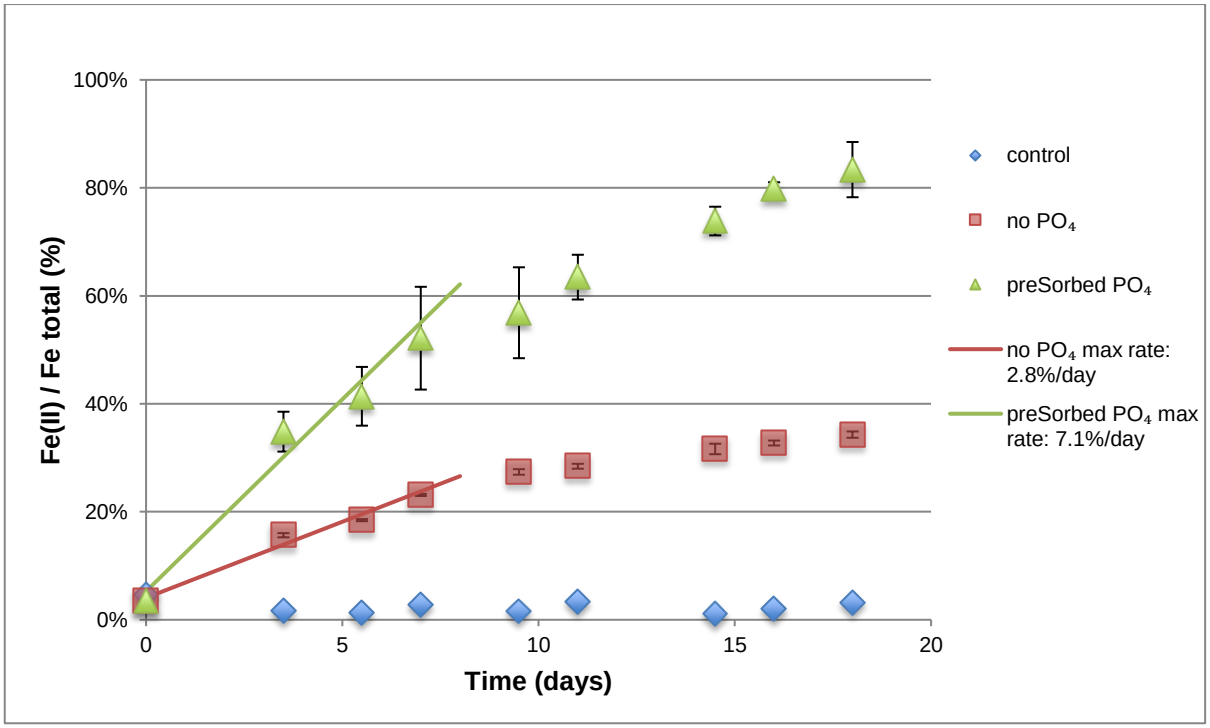

Figure 6. Reduction of Fe(III) to Fe(II) by *S. putrefaciens* over time. The co-precipitate with adsorbed phosphate was reduced much faster and to a greater degree of completion than with no adsorbed phosphate.

When phosphate had not been sorbed to the co-precipitate in advance of the reduction, the maximum rate or reduction was 1.9% per day, and when phosphate had been pre-sorbed to the iron oxide, the maximum rate of reduction was 7.3%/day.

3.3.2 *Eh, pH, and bacterial enumeration*

The redox potential (Eh), pH, and amount of bacteria (colony-forming units, or CFU) were tracked over the course of the reduction experiments. Figures for these measurements are presented in the Appendix.

Overall, the redox potential in microcosms containing *S. putrefaciens* started out positive (just above 100 mV), but dropped to negative potential values within 1-2 days and plateaued soon after, as seen in Figure A4. Organic carbon did appear to influence the changes in redox potential, causing it to become much more negative in the second reduction carried out on the co-precipitate. Pre-adsorbed phosphate also appeared to have a slight influence on reduction potential, also causing a further decrease.

The pH also appeared to be impacted to a certain extent the presence of organic carbon, as seen in Figure A5. Trials containing the co-precipitate exhibited an increase in pH over time, while trials without carbon (pure ferrihydrite) showed a slight decrease in pH but stayed relatively constant over time. It is not clear whether the presence of pre-adsorbed phosphate onto the iron oxide affected pH fluctuations over the course of the reduction experiments.

The amount of bacteria in each microcosm did not seem to change dramatically over time, as seen in Figure A6. It is expected that the numbers would eventually begin to decrease over time if sampling had continued for a longer period, which is observed to a small extent in trials containing the co-precipitate (at the very end of the experiment around day 18). No definitive trend was observed between trials with and without organic carbon, nor between trials with and without pre-adsorbed phosphate.

3.3.3 *Secondary mineral formation*

One of the objectives of carrying out the reduction experiments with iron-reducing bacteria was to determine the mineralogy of the post-reduction solids. After iron reduction had reached a plateau as determined by Fe(II) colorimetric absorbance readings at each sampling time interval, sediments remaining in the microcosms were rinsed several times with deoxygenated water inside the anaerobic chamber and left to dry. Secondary minerals were characterized by analysis of X-ray diffraction patterns and by scanning electron microscope. Table 2 below describes the post-reduction secondary minerals that were dried and ground for further analysis.

Table 2. Description of samples analyzed post-reduction.

Sample/trial	Pre-reduction microcosm contents	Post-reduction
1-C	Control from first reduction containing pure ferrihydrite	Ferrihydrite
1-1	Pure ferrihydrite, low phosphate	Goethite
1-2	Duplicate of 1-1	Goethite
1-3	Pure ferrihydrite, with pre-adsorbed (high) phosphate	Green rust
1-4	Duplicate of 1-3	Green rust
2-C	Control from second reduction, 10% C co-precipitate	Ferrihydrite
2-1	Co-precipitate, low phosphate	Ferrihydrite
2-3	Co-precipitate, with pre-adsorbed (high) phosphate	Vivianite

3.3.3.1 *X-ray diffraction*

All five dried and ground post-reduction samples from the first reduction (pure ferrihydrite) were analyzed with the X-ray diffractometer. Since the data gathered from both sets of duplicate trials (1-1 and 1-2, 1-3 and 1-4) were nearly identical, only the control (2-C) and samples 2-1 and 2-3 were analyzed from the second reduction experiment that used the co-precipitate (three total). Figure 7 shows the diffraction patterns of the samples from the first reduction experiment using pure ferrihydrite. In this figure, simplified graphs from published pure mineral data showing characteristic peaks were included below the collected data from this experiment. Experimental samples were determined to contain primarily one mineral, and possibly small amounts of other minerals based on additional peaks. Since no contamination of the control microcosm was observed during the reduction experiments, the diffraction pattern from the control in Figure 7 corresponds to that of ferrihydrite, as predicted. Samples 1-1 and 1-2 are nearly identical, and have a strong resemblance to diffraction peaks produced by goethite. Samples 1-3 and 1-4 are also very similar, and appear to primarily contain green rust, as well as some ferrihydrite. Figure 8 contains reference XRD data for green rust as collected by Parmar et al. (2001). A peak at 78° in sample 3 may indicate the presence of akaganeite, which exhibits a peak of relatively low intensity at this location, or the presence of magnetite, which has a peak of medium intensity at around 78°, as seen in additional reference XRD data displayed in Figure 10. There is also a possibility that this peak may result from interference from the sample holder.

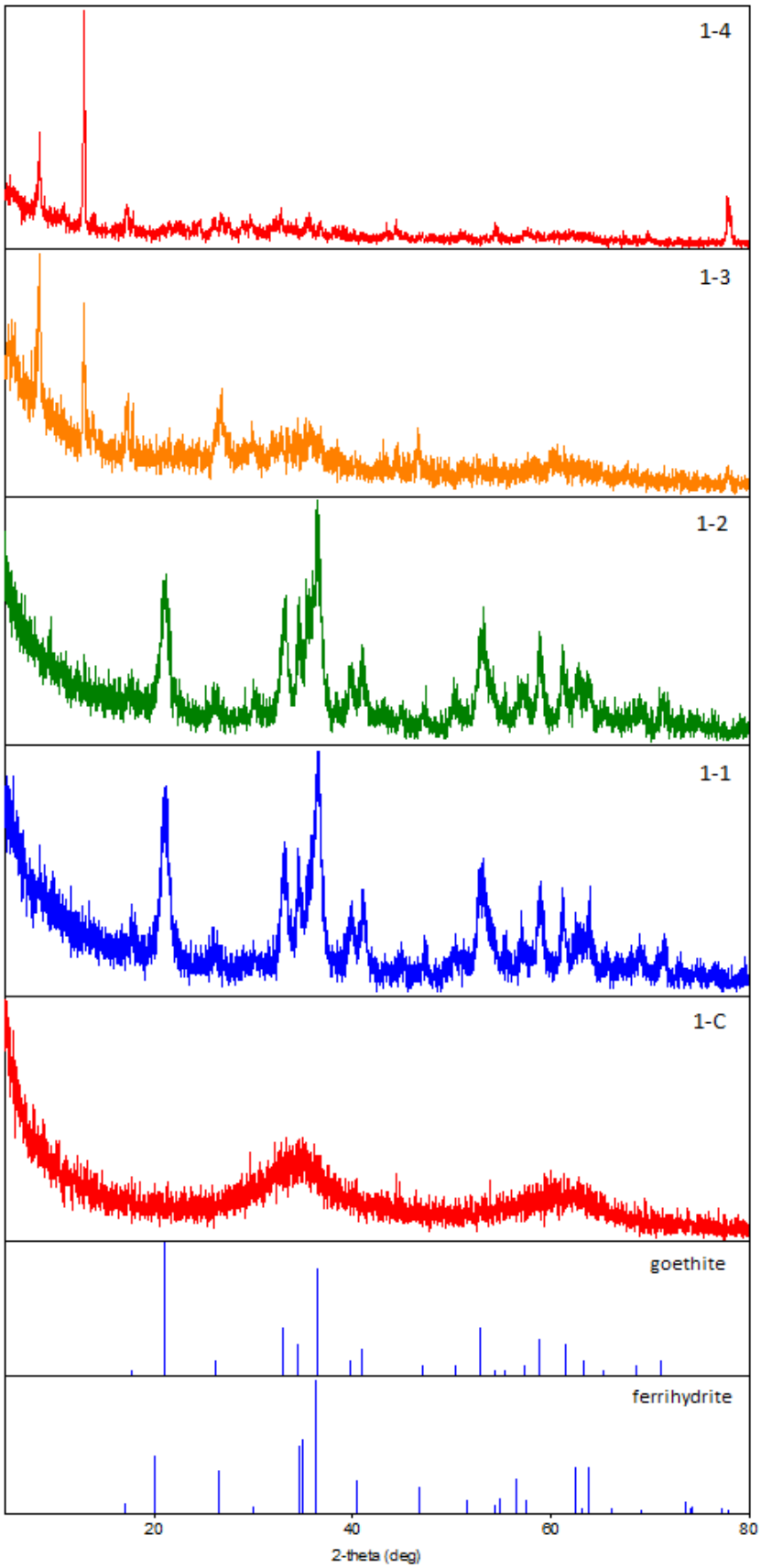

Figure 7. X-ray diffraction patterns collected for all five post-reduction samples from the first reduction experiment with pure ferrihydrite and *S. putrefaciens*. The two sections beneath the diffraction patterns are the characteristic peaks from reference data of pertinent minerals, for the purpose of comparison.

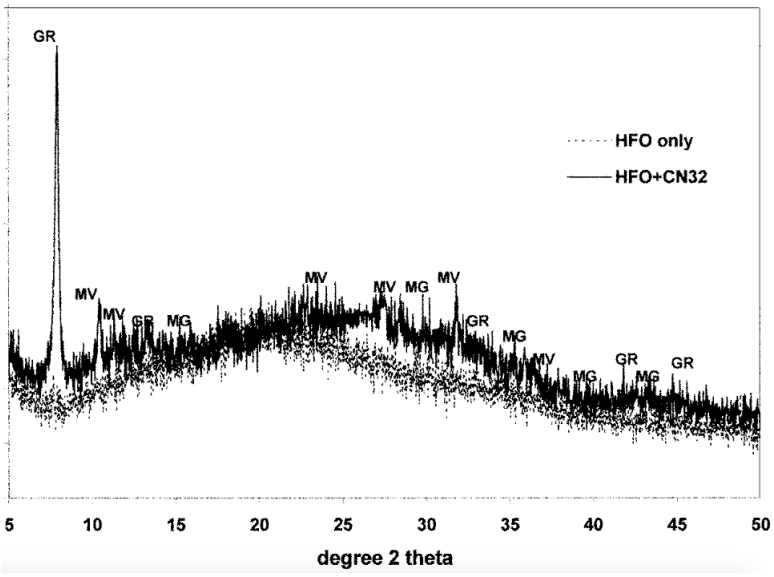

Figure 8. X-ray diffractograms of HFO and residual solids remaining after 30 days in a culture of *Shewanella putrefaciens* strain CN32 (Parmar et al. 2001).

The diffraction data collected from three of the five post-reduction samples in the microcosms containing alginate co-precipitates are presented in Figure 9. Since duplicates 1-1 & 1-2, and 1-3 & 1-4 in the first reduction appeared to be very similar during analysis, diffraction data from just one of each duplicate was collected for the resulting secondary minerals from the second reduction experiment. The control in the second reduction once again appears to contain only ferrihydrite, as seen in Figure 9. The presence of organic matter does not appear to influence the overall shape and location of the two primary peaks, although the intensity of peaks in sample 2-C is somewhat weaker than 1-C in Figure 7. Sample 2-1 (no pre-adsorbed phosphate) exhibits its most intense peaks near 21°, 36°, 44°, 62°, and 78°, indicating that it is likely made up primarily of ferrihydrite, and therefore did not appear to greatly change form. Sample 2-3 in Figure 9 appears to be almost entirely vivianite, with one large peak around 13° and a series of very small peaks between 20° and 50°.

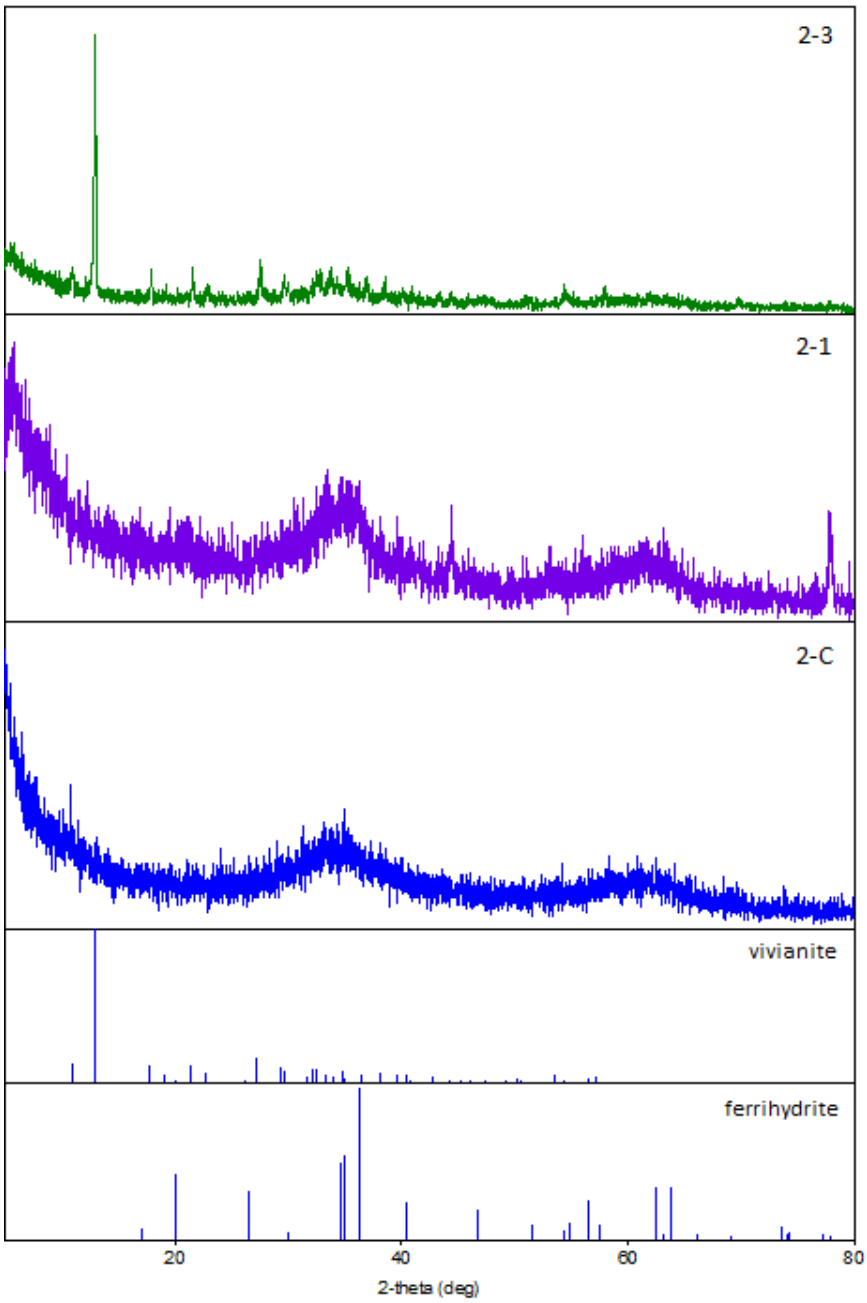

Figure 9. X-ray diffraction patterns collected for three post-reduction minerals formed from the second reduction experiment with ferrihydrite-alginate co-precipitate and *S. putrefaciens*. The two sections beneath the diffraction patterns are the characteristic peaks from reference data of minerals that are thought to be components of the experimental samples. They are included for comparison to the collected data.

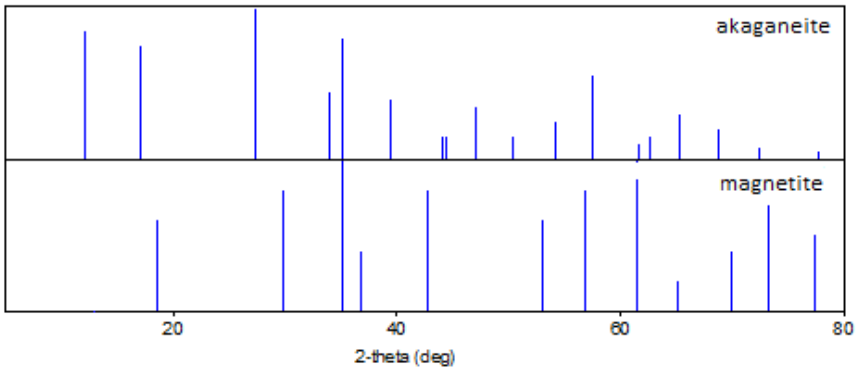

Figure 10. Reference data for two common iron oxide minerals, akaganeite and magnetite. Both exhibit peaks at key locations that may match peaks at some of the collected data in from this project, possibly indicating possible presence in smaller amounts. This reference data was gathered from the International Centre for Diffraction Data (ICDD) powder diffraction file (PDF) database.

3.3.3.2 *Scanning electron microscopy*

Micrographs were collected for post-reduction samples from the first reduction experiment, which used pure ferrihydrite, via SEM. Due to constraints pertaining to instrument availability, only the samples from the first reduction experiment with pure ferrihydrite were analyzed. For this reason, all secondary minerals formed post-reduction were mainly characterized via XRD. Figure 11 is a microgram of the post-reduction control from this study, thought to contain ferrihydrite. The particles appear to have sharp edges, although ferrihydrite is known to form in aggregated spherical particles (Jambor and Dutrizac 1998). Figures 12 and 13 are micrographs of the secondary minerals formed from ferrihydrite reduction by *S. putrefaciens*, and are thought to primarily contain goethite and green rust, respectively. The particles in Figure 12 appear to be round, amorphous clusters, although goethite is known to form in aggregations of rhomboidal columns (Bijani et al. 2016). The particles observed in Figure 13 appear to be flat and polygonal, which aligns with the findings of Parmar et al. (2001), who observed particles of thin, hexagonal plates in green rust micrographs.

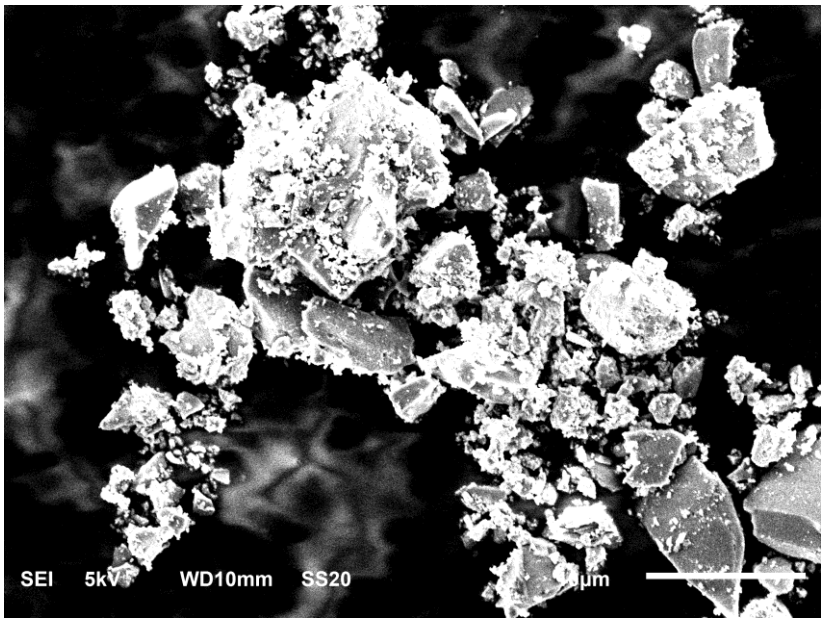

Figure 11. SEM image showing the post-reduction solids from the control of the first reduction experiment, containing no pre-adsorbed phosphate and no bacteria.

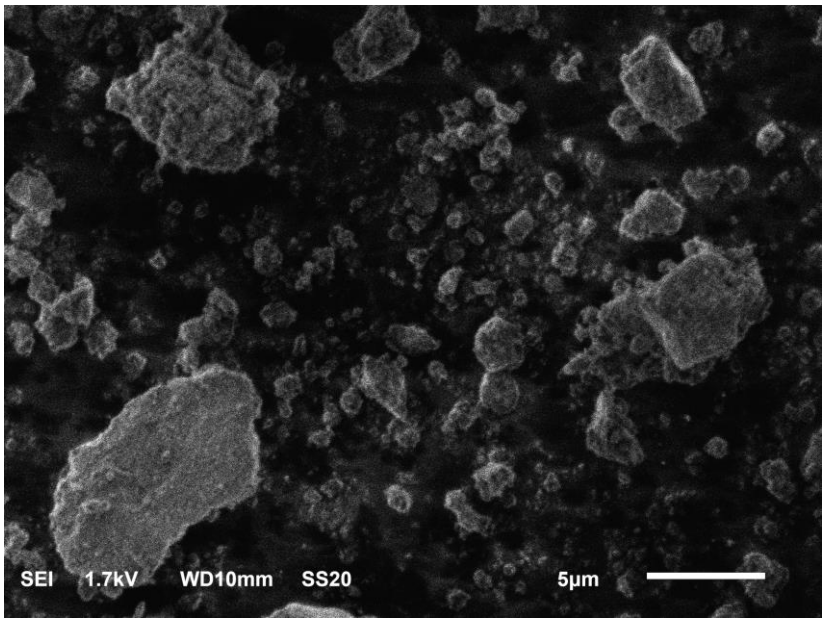

Figure 12. SEM image showing the post-reduction solids from sample 1-1 of the first reduction experiment, which initally contained only ferrihydrite and bacteria.

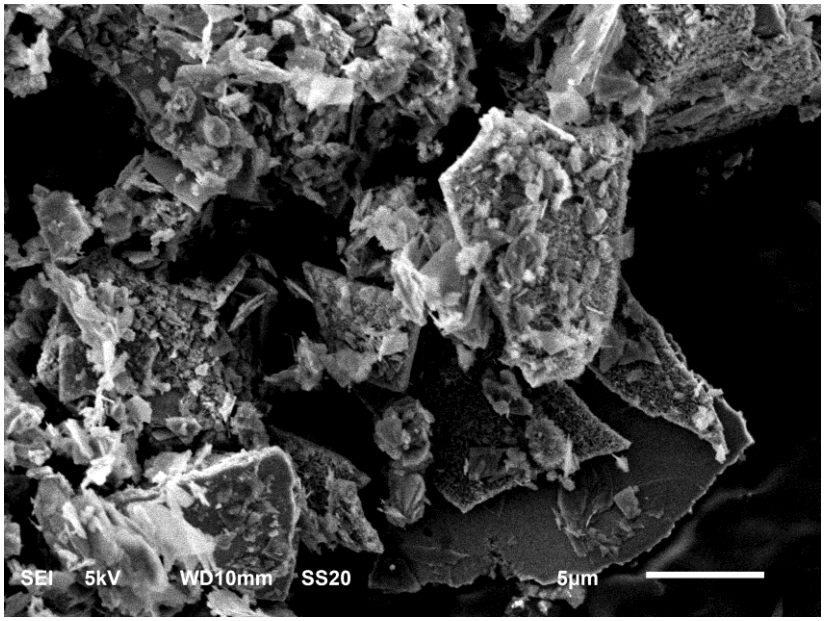

Figure 13. SEM image showing the post-reduction solids from sample 1-3 of the first reduction experiment, which initially contained ferrihydrite with pre-adsorbed phosphate, and bacteria.

3.3.4 *Fate of phosphate during bacterial reduction*

The fate of phosphate during the various reduction experiments is of central importance to this project. Figure 14 shows the release of soluble phosphate in the reduction microcosm containing pre-adsorbed phosphate onto ferrihydrite and alginate co-precipitates. Measurements were collected via ICP-MS over the course of the second reduction experiment only (containing organic carbon), while the initial and final concentrations were collected for the first reduction experiment (pure ferrihydrite). The initial concentration of free phosphate in both experiments is approximately 0.05 mM; much of the phosphate in the system is adsorbed to the surface of the iron oxide. Once the microcosms are inoculated, the free phosphate concentration in the second reduction experiment sharply increases to 0.1 mM after 5 days, and then drops to around 0.01 mM over time, plateauing at this level by the end of the experiment. This indicates that phosphate is being incorporated into post-reduction minerals that formed via bacterial reduction of ferric iron.

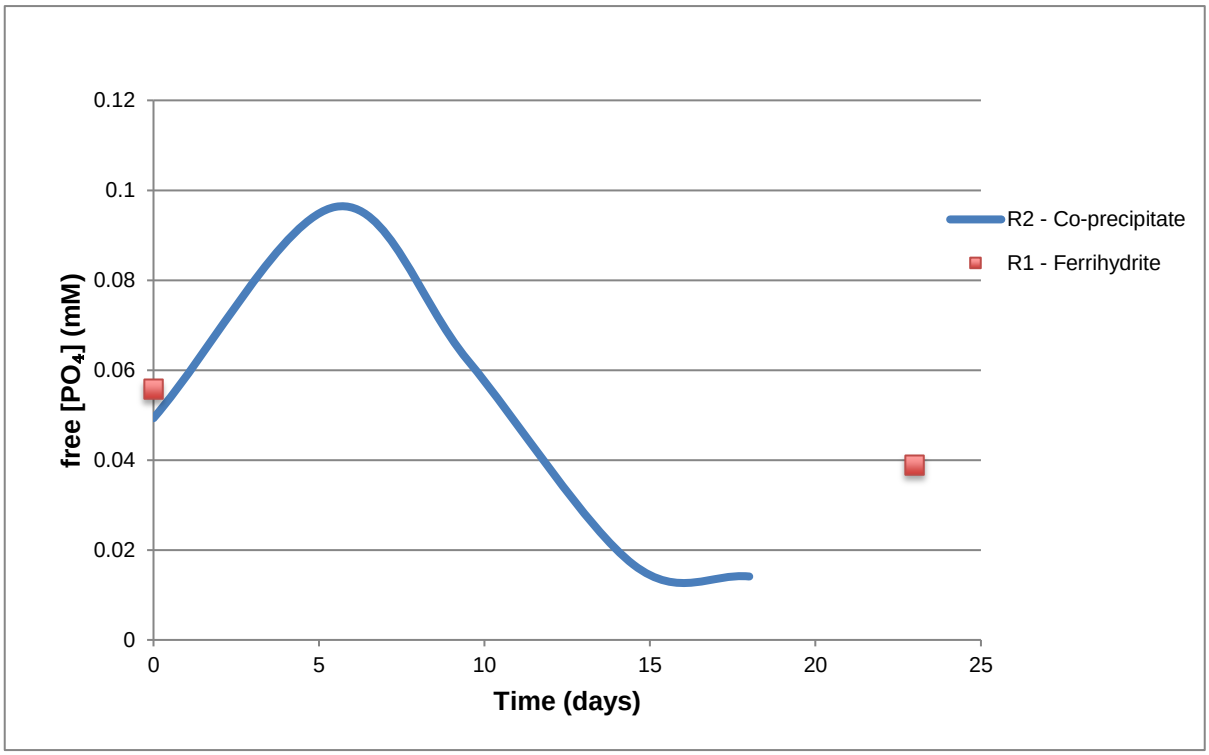

Figure 14. The concentration of free phosphate over time in the soluble phase of microcosms containing iron oxide with pre-adsorbed phosphate.

4. Discussion

The purpose of this project was to further assess the effectiveness of biogenic iron oxides for use in water treatment applications pertaining to the removal of excessive phosphate. This involved the use and synthesis of a laboratory model that is meant to be analogous to natural biogenic iron oxides in order to determine whether the presence of organic matter made a significant difference on the ability of the iron oxide to sequester phosphate.

Since ferrihydrite is a prevalent, naturally occurring, amorphous mineral that is frequently formed by iron oxidizing bacteria (Schwertmann and Cornell 2000), its use for water treatment in areas where it is naturally found could pose a simple and cost-effective solution to certain types of pollution. Knowledge of the conditions under which iron oxides can adsorb the maximum amount of an anion such as phosphate is key to the development and/or improvement of remedial technologies. Similarly, a thorough understanding of the fate of phosphate in locations where iron-reducing bacteria exist is important in the context of the potential for phosphate to desorb after reductive dissolution.

4.1 *Properties of iron oxides*

In the laboratory model of alginate coprecipitated with ferrihydrite, the alginate causes the resulting substance to become more and more gelatinous in texture with progressive increases in the ratio of carbon to iron. The coprecipitated alginate simulates the texture and organic content of the exopolysaccharides excreted from iron-oxidizing bacteria, and the synthesis of samples with different amounts of organic carbon is meant to be analogous the natural variance of conditions in the aquatic systems in which biogenic iron oxides are formed by iron oxidizing bacteria. For example, several natural BIOs samples collected from Duhamel, Québec were found to have an organic content of 21-24%, based on loss on ignition (LOI) analysis, and samples collected from New Calumet Mine had an organic content of 13-27% (M. Moriarty, personal communication). By comparison, co-precipitated samples synthesized in-laboratory were found to have 21-33% organic content.

The points of zero charge of pure synthetic ferrihydrite and the synthetic co-precipitate with 4% carbon were determined at pH 7.2 and 6.4 respectively. Zeta potential measurements on samples with higher organic content were attempted, but the results obtained yielded entirely negative values within the pH range examined, as seen in Figure 1 with the green points representing a sample with 6.5% carbon. The lowest pH tested was pH 4, due to the solubility of ferric iron around pH 3.5 - 4 (Schwertmann 1991). This suggests that organics have a significant effect on the surface charge of iron oxides. A study conducted by Schwertmann and Fetcher (1982) on the determination of the pH_{zpc} for both synthetic and natural samples of ferrihydrite reported values for synthetic iron oxides that usually fall between pH 7 and 9, whereas the pH_{zpc} values of six natural iron oxides were between pH 5.3 and 7.5 due to presence of silicates and/or organic matter. Those findings match the results from this study, where an increase in the C/Fe ratio of the co-precipitates causes the zeta potential measurements to become increasingly negative, as seen in Figure 1.

4.2 *Adsorption*

4.2.1 *Summary of results*

Synthetic co-precipitates were tested for their adsorption capacity of phosphate. It was found that for the range of carbon content of the co-precipitates examined in this study, the amount of alginate did not appear to affect the degree of adsorption of phosphate that occurred. It was predicted that the alginate would act as a barrier between the positively charged binding sites on the surface of the iron oxides and prevent adsorption of phosphate ions, decreasing the efficiency of sorption (S_{max}) with an increasing ratio of organics. It was also hypothesized that pure ferrihydrite would be a much more potent adsorbent than the coprecipitates. Interestingly, pure ferrihydrite did not have the highest adsorption capacity among the trials. It is possible that the reason for this is that the positive surface charge is maintained by the organic matter and so anions are able to adsorb to the co-precipitate surface with a similar affinity. It is also possible that any expected blocking effect from the presence of high amounts of organic matter is negated by a significant increase in surface area as a result of this increase. The synthetic iron oxides were found to be a relatively good model for natural biogenic iron oxides, as seen when comparing the graphical representations of the adsorption kinetics

of the natural samples (Figure 3) with the synthetic samples in Figure 2. Data points in Figure 2 (yellow) from one of the natural samples, CA-02 was included to demonstrate that its adsorption capacity fell within a similar range as those of synthetic samples. Adsorption maxima from the natural samples were slightly lower overall than laboratory-prepared samples. This was expected, as natural samples are likely to contain a wealth of other compounds. A study that assessed the impact of humic substances on the phosphate adsorption of metal oxides found that their presence had limited effects on the adsorption of phosphate, and that any potential difference in the amount of phosphate adsorbed was eliminated as equilibration time was extended (Borggaard et al. 2005). Although humic and alginic acids do not necessarily produce the same results, these findings were comparable with respect to the lack of impact of organic matter on adsorption observed in this study.

4.2.2 *Comparisons with other studies*

A study that examined the potential for removal of phosphorus from solution using biogenic iron oxides (Rentz et al. 2009) carried out similar adsorption experiments on BIOS collected from four sites in a wetland adjacent to Moose Creek Reservoir in Idaho, USA. The authors found that the maximum adsorption of phosphorus per unit iron was 47 - 165 mg P/g Fe, which was normalized to the total Fe content. For the samples analyzed in this project, the maximum adsorption of phosphorus per unit iron was determined to be 57 - 131 mg P/g Fe (also normalized to total Fe), which fully falls within the range of the adsorption capacity of the Moose Creek wetland BIOs. When comparing the results in this project to the Moose Creek published values, care was taken to ensure that S values (amount of phosphate adsorbed per unit adsorbent) were converted from the units of mg PO_4/mg Fe to mg P/g Fe. The Moose Creek study compared its maximum adsorption results to other studies that also carried out phosphorus adsorption analyses on iron-rich substrates, including brick coated with iron oxide (Boujelben et al. 2008), a synthetic gypsum-iron oxide material, and iron oxide coated sand (Del Bubba et al. 2003, Arias et al. 2006, Boujelben et al. 2008). Maximum P adsorption in each of these studies fell within the range of the Moose Creek study, and none of them were described by authors as having a biological origin. This demonstrates the favourable adsorption capacity of iron oxides produced biotically via

bacterial oxidation (Rentz et al. 2009). Though these two types of iron oxides have been generally found to have relatively equal effectiveness, the use of a biological adsorbent with minimal or no preparation needed over a specially manufactured material presents an economic advantage.

An investigation carried out in Korea assessed the use of several iron oxides (abiotically produced) as adsorbents for phosphorus in wastewater (Kang et al. 2003). The adsorptive capacity of ferrihydrite, goethite, and hematite were examined. Interestingly, in the Kang study, it was found that pure ferrihydrite particles had a maximum adsorption 'S' of approximately 30 mg P/g Fe, which is significantly lower than the 68 mg P/g Fe that was determined as the maximum adsorption for pure ferrihydrite in this project. It should be noted that in the Korean study, phosphate solution was left to equilibrate with the adsorbent for 30 minutes, while in this project, adsorption was carried out for 48 hours. The kinetics do not fully account for this discrepancy, with this project determining that 71% of phosphate adsorption occurs within 30 minutes and 88% adsorbed after 48 hours, reaching a plateau in adsorption around 96 hours (assumed to be approaching maximum). The Korean study also compared the adsorption capacity of goethite and hematite, which are more ordered iron oxide minerals. It was found that ferrihydrite had a much greater adsorption capacity for phosphate than goethite and hematite, which exhibited maximum adsorption of approximately 4.5 and 2.5 mg P/g Fe respectively. This difference is likely due to the fact that ferrihydrite has a much greater surface area per unit mass than the surface area of these two more ordered minerals.

Comparisons of other adsorbents are usually reported as normalized to solids. Since iron oxides have such a wide range of iron content per unit mass, especially the laboratory models in this project with varying amounts of organics, a generalization of iron oxides' maximum adsorption capacity with respect to solids does not carry much meaning. The procedures and data processing were carried out in this project in a similar way to the Moose Creek study (Rentz et al. 2009), and the adsorption capacity results normalized to iron were comparable. Therefore the reported values from Rentz et al. for maximum adsorption capacity of biogenic iron oxides normalized to solids (11 - 40 mg P/g) will be used to compare the efficacy of biogenic iron oxides to other

adsorbents in the subsequent paragraphs.

Aluminum oxides have been similarly studied and were found to have decent sorptive capacity for phosphate. A study in Japan (Tanada et al. 2003) determined the maximum adsorption capacity of aluminum oxides to be approximately 11 mg P/g of aluminum hydroxide solids, (authors reported as 35 mg PO_4/g, converted for the purpose of this comparison), which just falls within the range of 11 - 40 mg P/g biogenic iron oxide. Another study assessing the phosphate sorption capacity of different oxide minerals confirms that aluminum and iron oxide minerals do not exhibit a noticeable difference in sorption capacity (Goldberg and Sposito 1984).

The mineral calcite ($CaCO_3$) has been tested for adsorption capacity, and has been found to be an effective adsorbent for phosphate. Though the sorption of phosphate to calcite is also pH-dependent, its adsorption capacity increases as pH increases, the opposite phenomenon observed for iron oxides (Karageorgiou et al. 2007). This is likely due to increasing solubility of the mineral as pH decreases from neutral to acidic conditions. At pH 12 it was noted that 100% of phosphate sorption took place in a system containing 1 g calcite and 20 ppm phosphate. No direct comparison was made between the effectiveness of calcite as a sorbent and of biogenic iron oxides of this project because of the low ratio of phosphate to adsorbent used in the Karageorgiou study. In terms of practicality, however, it is interesting to note that in a contaminated area under basic conditions where iron oxide would not be an effective adsorbent, calcite could potentially be used to remove phosphate.

An Australian study that focused on maximizing adsorption conditions in constructed wetlands carried out an analysis of the phosphate adsorptive capacity of several materials, including soil, blast furnace slag (an industrial byproduct), and zeolite, an aluminosilicate mineral that is widely used as an adsorbent and for uses in water purification (Sakadevan et al. 1998). The most effective adsorbent was found to be the blast furnace slag, with a reported maximum sorption capacity of 44.2 g P/kg slag, the unit being equivalent to mg P/g slag, which is comparable on the higher end of the range of values of iron oxides identified in this project, 11 - 40 mg/g.

As phosphate pollution has become more of an environmental issue in the past few decades, the need to develop new remediation systems has become known. Lanthanum in particular has attracted attention due to its lack of toxicity and its high affinity for phosphate. Activated carbon fibre doped with lanthanum oxide is an example of an adsorbent that has recently been created and tested (Zhang et al. 2012). Maximum sorption capacity for this material was found to be 15.3 mg PO4/g, comparable to the effectiveness of iron oxides. It has been found to be very chemically stable and physically strong, but the cost of materials and effort of synthesis give it a disadvantage over naturally occurring biogenic iron oxides.

4.3 *Microbial reduction and the fate of phosphate*

4.3.1 *Rates of reduction*

4.3.1.1 *Summary of rates*

The reduction experiments were carried out for a number of reasons. One was to examine the difference in rates of reduction with and without alginate, and with and without phosphate adsorbed to the surface of the iron oxides. Between pure ferrihydrite and the 10% C co-precipitate (and without having pre-adsorbed phosphate), the maximum reduction rates were 2.8% and 1.9% reduction per day, respectively. In the trials where phosphate was fully covering the surface of the iron oxides, the maximum rates of reduction with pure ferrihydrite and the co-precipitate were 7.1% and 7.3% respectively. The presence of alginate does not appear to have an effect on the rates of reduction. The presence of phosphate, on the other hand, does noticeably increase the rate of reduction of ferric iron to ferrous iron in the presence of *S. putrefaciens* CN32. This is very likely due to phosphate's pivotal role in the regulation of metabolic processes. The formation and hydrolysis of high-energy phosphate bonds make up the majority of energy storage and release within all organisms (Blake et al. 2005), and as such, its availability can dictate their rate of growth.

4.3.1.2 *Comparison to similar studies*

With respect to other studies that have observed the rates of reduction of ferric iron under similar conditions, rates from this project are in some cases comparable to

published values, but in other cases, they were found to be different. A recent study observed that phosphate at a concentration of 3.9 mM in solution increased the rate (6.5%/day) of ferric iron reduction, as well as the total extent of reduction (91%), compared to conditions containing 10 μM phosphate, which showed a maximum rate of 5.4%/day and a total extent of 40% reduction of Fe(III) overall (Najem et al. 2017). An earlier study also found that the anaerobic reduction of 2-line ferrihydrite in the presence of 3.9 mM phosphate enhanced both the extent and the rate of reduction, and initiated the formation of green rust and vivianite as secondary minerals (Fredrickson et al. 1998). A study that also examined the rates of reduction of ferrihydrite with differing amounts of phosphate showed conflicting results. Three treatments containing 4 mM phosphate exhibited initial rates of reduction of 0.4%, 2.1%, and 3.6% per day, and a treatment containing 0.4 mM had a rate of 0.5% reduction of Fe(III) to Fe(II) per day. It should be noted that these studies did not pre-adsorb phosphate to the iron oxide before carrying out the reduction experiment, as it was done in this project. Other potential differences in methodology among studies could account for this range of results.

4.3.1.3 *Impact of organics*

The effect of organic matter on reduction rates in this project was not observed to have an impact. In low phosphate conditions, pure ferrihydrite was initially reduced by 2.8%/day and 1.9%/day for the co-precipitate, while in conditions of high phosphate, pure ferrihydrite was reduced by 7.1%/day, and the OM sample 7.3%/day. Interestingly, Shimizu et al. (2013) found that when they varied the C/Fe ratio in coprecipitates and performed bioreductions on the synthetic samples, low ratios of C/Fe (<0.8) slowed down the reduction, and high ratios (>1.8) increased the rate. The C/Fe ratio of the co-precipitate used in this project was determined to be approximately 0.85 (10% C dry weight), which by chance falls within the 'middle' ground between the two noted high and low ratios (Shimizu et al. 2003). The lack of effect of organic matter observed this project agree with the findings of Shimizu and colleagues. Their study found that the presence of organic matter inhibited the formation of minerals such as goethite and magnetite in favour of green rust, which was also observed in this project.

4.3.1.4 *Impact of phosphate*

The elevated rate of reduction within microcosms containing high phosphate can be attributed to the greater amount of available phosphate that can be used by the organisms for metabolic processes. This theory is supported by the bacterial counts that were tracked throughout the reductions. In both experiments, the microcosms containing pre-adsorbed phosphate exhibited a greater spike in bacteria colony-forming units than in microcosms (Figure A6), indicating that their environments were nutrient-rich and promoted growth more so than the microcosms with very low phosphate.

Similarly, Figure 14 shows the concentration of free phosphate in solution over time throughout the second reduction experiment. The concentration spikes from the initial amount within 5 days of inoculation, likely due to microbial activity causing the phosphate ions to de-sorb. As the reduction progresses, secondary minerals begin to form. Some of the free phosphate precipitates out of solution becomes bound to the solids or gets incorporated into the matrix of the minerals being formed. The final concentration of free phosphate in solution was observed to be lower than the initial concentration.

The correlation of higher free phosphate and faster reduction appears to behave like a positive feedback loop: more phosphate is present in the microcosms in which phosphate has been pre-adsorbed to the iron oxides, so bacteria thrive and function optimally due to high nutrients. This results in more iron being reduced, and the decrease in surface charge from 3+ to 2+ displaces more adsorbed phosphate off the iron oxide surface into solution. This speculative assertion is based solely on Figure 14, which tracks free phosphate concentration over time in the reduction experiment containing iron oxide co-precipitated with organic matter. Because of this, it is assumed that the secondary mineral that is formed uses the free phosphate in solution. However, it is also possible that the biomineralization process uses adsorbed phosphate instead of free phosphate.

Even though the reduction of ferric iron to ferrous iron results in a decrease in net surface charge, it is assumed that some of the adsorbed phosphate remains attached to

the mineral surface despite the decrease in net positive charge. Regardless, since the final concentration of free phosphate is lower than the initial concentration, this knowledge is beneficial for practical applications. It had been initially hypothesized that after reduction of ferric iron to ferrous iron via iron-reducing bacteria, much of the adsorbed phosphate would be released into solution due to the change in surface charge. If this had been the end of the process, then any attempt at employing ferric iron oxides to sequester excess phosphate in an environment where iron-reducing bacteria are present would be fruitless if phosphate simply de-sorbed back into solution when ferric is reduced to ferrous. The observed incorporation of phosphate into secondary minerals and of observed decreases in concentrations of free phosphate by the end of the experiment indicates that remedial efforts of using iron oxides to remove phosphate from nutrient-polluted waters could be successful even in the presence of iron reducing bacteria.

4.3.2 *Secondary mineral formation*

As acknowledged in the introduction, reduction of ferric iron oxide minerals by iron-reducing bacteria generally results in the precipitation of new minerals, depending on the chemical conditions. Within both reduction experiments

4.3.2.1 *X-ray diffraction data*

Based on the X-ray diffraction data collected from the secondary minerals, it is likely that the main reason for the drop in concentration of free phosphate by the end of the reduction is because much of it is being crystallized with ferrous iron and incorporated into the structure of the mineral. Green rust has been known to form under conditions where phosphate is present (Fredrickson et al. 1998, Kukkadapu et al. 2004). It appears to be major component of post-reduction solids in the reduction trial that initially contained pure ferrihydrite and pre-adsorbed phosphate. An intense peak at 8° can be observed in the top section of Figure 7 labeled 1-1, as outlined in section 3.3.2.1. This bears a close resemblance to the XRD data for green rust (Figure 8) collected from a similar study (Parmar et al. 2001).

Vivianite has a chemical structure of $Fe_3(PO_4)_2 \cdot 8H_2O$. The two phosphate molecules each have a charge of 3-, which corresponds to three ferrous iron ions each having a charge of 2+. Vivianite X-ray diffraction data has one intense characteristic peak at 13° along the 2θ x-axis, with few other notable features. The post-reduction mineral sample from microcosms containing the 10% C co-precipitate with pre-adsorbed phosphate produced X-ray diffraction patterns that were strikingly similar to published diffraction data of pure vivianite. The top section labeled 2-3 of Figure 9 contains one peak of high intensity at 13°, comparing closely to reference data for vivianite, which is located near the bottom section of Figure 9. It should be noted that the sample holder used in this analysis can produce peaks at the following angles: 38.2°, 44.5°, and 77.9°, therefore certain peaks near these locations may be attributed to interference.

Both the presence of organic matter and saturation of phosphate did appear to have an effect on the secondary mineral formation. Four different minerals formed consistently among duplicates of the four different treatments. Figure 15 below shows a simplified quadrant graphic of the most significant mineral determined to be present post-reduction within each set of conditions.

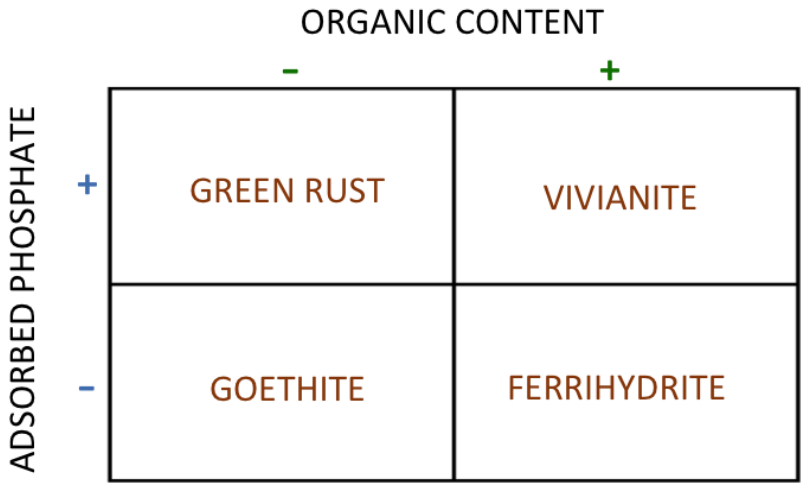

Figure 15. A visual representation of the majority component of the secondary mineral formation observed by X-ray diffraction in each set of conditions examined in the iron-reducing bacteria experiments.

In the low-phosphate microcosms, the absence of this nutrient had a significant effect on the total reduction that occurred. Pure ferrihydrite was 34% reduced, and the co-precipitate was 42% reduced. In both cases, the resulting mineral appeared to be primarily ferric in composition, with goethite being formed from pure ferrihydrite. In the second reduction experiment that contained the co-precipitate, the XRD pattern for the secondary mineral formed in microcosm 1 (conditions outlined in table 2) appears to contain mainly ferrihydrite. The lack of change observed in the microcosm containing low phosphate and high organic carbon could indicate that alginate partially blocked access of bacteria to the iron oxides, especially when the bacteria were not well nourished.

In high phosphate conditions, on the other hand, 83% reduction occurred with pure ferrihydrite, and 86% reduction occurred for the co-precipitate. If alginate does indeed create some sort of blocking effect, the high phosphate conditions would appear to negate this.

The presence of alginate in the high phosphate trials of the second reduction resulted in the formation of vivianite, while its absence produced green rust. The complex interactions between organic matter, inorganic compounds, and microbes control the reduction pathway of iron, but it is not always clear how. The formation of both vivianite and green rust during iron oxide reduction under conditions with high phosphate is discussed at great length in a number of papers, particularly in a study by Borch and colleagues (Borch et al. 2007). No mention was made on the difference in mineralization pathways or the effects of different compounds in the formation of vivianite over green rust and vice versa, but the results from this project suggest that the presence of organic carbon favours the formation of vivianite. O'Loughlin and colleagues report that the reduction of iron oxides usually results in the formation of the minerals magnetite, siderite, and vivianite, and that green rust is generally only found as a product of ferrihydrite or lepidocrocite reduction (O'Loughlin 2007).

4.4 *Applications and practical considerations*

A recent study in China (Li et al. 2015) explored the use of extracellular polymeric substances, or exopolysaccharides (EPS) as a biological method of phosphorus removal. A major element of this review is that it had been conventionally believed that phosphorus-accumulating organisms (PAOs) that take up significant amounts of P from solution transform the P atoms into polyphosphate and store it within the cell. Novel research has found that the EPS plays a major role in the uptake of P, acting as a reservoir (Zhang et al. 2013). Though the authors make no mention of iron oxidizing bacteria when describing PAOs, it is widely known that iron oxidizers such as species of *Leptothrix* and *Gallionella* excrete exopolysaccharides in the form of sheaths or stalks that surround their cell walls (Fortin and Langley 2005). This could represent a 'double dividend' for the bioremedial potential of some types of bacteria: the oxidation of ferrous iron to ferric iron oxides, resulting in a potent sorbent for phosphate; and the possible uptake of phosphate into the exopolymeric material of the microbe.

If a treatment facility were to engineer a system that used iron to remove phosphorus from water, the designers might explore the benefits of using biogenic iron oxides, which could be more complicated, versus synthetic iron oxides, which may require fewer components and therefore might be more cost effective. The aforementioned Moose Creek study (Rentz et al. 2009) describes a scenario in which biogenic iron oxides may in fact be a more favourable option with respect to the 'rechargeability' of the apparatus. The sorptive capacity of an aggregate filter that contains iron-oxidizing bacteria and fed iron and oxygen can be regenerated via regular filter use once it has reached its maximum capacity for phosphorus adsorption. A periodic backwash of the filter would remove the saturated iron oxide, and re-supplying the filter and microbe community with solutions of iron and oxygen would allow the iron oxides to be replenished (Rentz et al. 2009). This process would be a sustainable way to extract and discard harmful concentrations of phosphate.

The Korean study previously mentioned (Kang et al. 2003) described its methods of regenerating the iron oxide particles used during experimentation. In one method, contents of the experimental tubes (containing iron oxides with bound phosphate

suspended in a solution containing the unadsorbed phosphate) were centrifuged and the supernatant was set aside for P content analysis. Sodium hydroxide, a strong base, was added to the iron oxide particles (pellet) and forcibly mixed for 5 minutes. This process was repeated and the iron oxides were neutralized before subsequent use. Interestingly, the authors also tracked the efficiency of phosphorus removal of the regenerated iron oxides after each use for fifteen cycles, and found that the efficiency of ferrihydrite began at 80% P removal and steadily decreased to around 35% P removal at the fifteenth cycle. This knowledge is useful and presents a potentially new line of inquiry for the development of a regeneration procedure that maintains close to the initial efficiency of adsorption.

A review that examines the adsorption efficiency of mesoporous materials (containing pores of 2 - 50 nm) also discussed a number of methods of regeneration for adsorbents after they had reached saturation of phosphate on surface binding sites (Huang et al. 2017). The application of sodium hydroxide solution can successfully remove all or nearly all bound phosphate on several adsorbents, including ammonium-functionalized mesoporous silica (Saad et al. 2007). Metal-doped mesoporous silicas were regenerated by allowing them to soak in nitric acid, although their sorption capacity decreased from this process (Ou et al. 2007). Synthetic iron and zirconium oxide particles were created as an adsorbent and were able to be repeatedly regenerated with potassium hydroxide solution while maintaining over 80% of its capacity (Sarkar et al. 2010). Determining methods of regenerating adsorption capacity of potential adsorbents is key for the implementation of remediation technologies. Additionally, adsorption as a method of phosphate removal allows for phosphate recovery & recycling, whereas traditional chemical methods do not (Huang et al. 2017).

5. Conclusion

5.1 *Summary of key findings*

The goal of this study was to contribute to the body of research pertaining to the use of iron minerals to reverse environmental pollution caused by human activity. Iron oxides have been found to be powerful adsorbents for phosphate but have not yet been put to use for large-scale water treatment projects. This project assessed the effects of different levels of organic matter within the iron oxide matrix on their adsorptive capacity of phosphate. This was done to simulate biogenic iron oxides, which are formed by iron-oxidizing bacteria and are prevalent in the environment. At the C/Fe ratios examined, organic matter did not appear to have a noticeable impact on phosphate adsorption to iron oxides. The effect of changes in pH on adsorptive capacity of iron oxides was also examined, and it was confirmed that the capacity increased with decreasing pH.

Reductions of iron oxides were conducted with *Shewanella putrefaciens* CN32. This was undertaken mainly to determine whether phosphate adsorbed to iron oxides would simply go back into solution when exposed to iron-reducing bacteria, thereby lessening the potential for effectiveness in water treatment in areas where these types of bacteria thrive. A comparison of reduction rates, extent of reduction, and post-reduction mineral formation was also conducted on both pure iron oxides and alginate co-precipitates, with and without phosphate adsorbed. It was found that co-precipitated organic matter does not appear to affect the rate or extent of reduction, but does affect the secondary mineralization, with ferrihydrite remaining the the major mineral in conditions of low phosphate and vivianite forming in conditions of high phosphate. Goethite and green rust tended to form after the reduction of pure ferrihydrite, under conditions of low and high phosphate, respectively. Phosphate adsorbed to the iron oxide surface before reduction was observed to have greatly increased the rate and extent of reduction of Fe(III) to Fe(II), and also had an effect on post-reduction mineralization. Importantly, it was found that pre-adsorbed phosphate was not just released back into solution after reduction, but incorporated into the newly precipitated minerals. This brings additional confidence to the practicality of using biogenic iron oxides for remediation.

5.2 *Potential next steps*

Further investigations within this topic could include a more comprehensive comparison of adsorption capacity as it pertains to the C/Fe ratio. This could be conducted by collecting %C data on a wider sampling of natural biogenic iron oxides, and then forming co-precipitates that match both the high and low of carbon content within and even beyond the range. The synthesis of a laboratory model helps isolate variables of interest and eliminates the influence of other potential components of natural samples (i.e. aluminum oxides). The regeneration capacity of biogenic iron oxides would also be a pertinent next step, assessing the effectiveness of some of the methods discussed in section 4.4 of this paper. Reproducing the reduction portion of this study with another type of iron-reducing bacteria such as G*eobacter metallireducens* may also present a worthwhile comparison.

The more attention that is dedicated to the remediation of lakes, rivers, and marine environments experiencing nutrient pollution, the sooner and more effectively these problems can be rectified. The use of naturally occurring and prevalent materials to carry out such tasks may be a cost-effective and sustainable endeavour. Though climate change and ocean acidification are extremely pressing environmental concerns, the protection of the quality of Earth's freshwater resources should also remain a priority.

References

Akob, D., Mills, H., Gihring, T., Kerkhof, L., Stucki, J., Anastaio, A., Chin, K., Kusel, K., Palumbo, A., Watson, D., Kostka, J. 2008. Functional Diversity and Electron Donor Dependence of Microbial Populations Capable of U(VI) Reduction in Radionuclide-Contaminated Subsurface Sediments. Applied and Environmental Microbiology 74(10): 3159-3170.

Arias, M., Silva-Carballal, J., Garcia-Rio, L., Mejuto, J., Nunez, A. 2006. Retention of phosphorus by iron and aluminum-oxides- coated quartz particles. Journal of Colloid and Interface Science 295, 65–70.

Baker, B., Banfield, J. 2003. Microbial communities in acid mine drainage. FEMS Microbiol Ecol. 44(2): 139-52.

Barron, V., Torrent, J., de Grave, E. 2003. Hydromaghemite, an intermediate in the hydrothermal transformation of 2-line ferrihydrite into hematite. American Mineralogist 88(11-12): 1679-1688.

Bazylinski, D., Heywood, B., Mann, S., Frankel, R. 1993. Fe3O4 and Fe3S4 in a bacterium. Nature 366(6452): 218.

Benitez-Nelson, C. 2000. The biogeochemical cycling of phosphorus in marine systems. Earth-Science Reviews 51: 109–135.

Bijani, S., Martinez, L., Dalchiele,E., Gabas, M., Schrebler, R., Ramos-Barrado, J. 2016. Surface Morphological Control of Nanostructured Single-Phase Fe3O4, α-FeOOH and γ-FeOOH Electrodeposited Thin Films. Journal of The Electrochemical Society 163(8): D366-D373.

Blake, R, O'Neil, J, Surkov, A. 2005. Biogeochemical cycling of phosphorus: Insights from oxygen isotope effects of phosphoenzymes. American Journal of Science 305(6-8): 596-620.

Borch, T., Masue, Y., Kukkadapu, R., Fendorf, S. 2007. Phosphate Imposed Limitations on Biological Reduction and Alteration of Ferrihydrite. Environ. Sci. Technol. 41: 166-172.

Borch, T., Kretzschmar, R., Kappler, A., Cappellen, P., Ginder-Vogel, M., Voegelin, A., Campbell, K. 2010. Biogeochemical redox processes and their impact on contaminant dynamics. Environ. Sci. Technol. 44(1): 15−23.

Boujelben, N., Bouzid, J., Elouear, Z., Feki, M., Jamoussi, F., Montiel, A. 2008. Phosphorus removal from aqueous solution using iron coated natural and engineered sorbents. Journal of Hazardous Materials 151, 103–110.

Bruun, A., Finster, K., Gunnlaugsson, H., Nørnberg, P., Friedrich, M. 2010. A Comprehensive Investigation on Iron Cycling in a Freshwater Seep Including Microscopy, Cultivation and Molecular Community Analysis. Geomicrobiology Journal 27(1):15.

Canecka, L., Bujdos, M., Boriova, K. 2015. Fe Oxo-Hydroxides and Their Potential Utilization in Reducing the Content of Some Undesirable Elements in the Natural Environment by Sorption Mechanisms. Chem.Listy 109(2): 105-108.

Carlson, L., Schwertmann, U. 1981. Natural ferrihydrite in surface deposits from Finland and their association with silica. Geochim. Cosmochim. 45(3): 421−429.

Chan, C.S.; Fakra, S., Edwards, D., Emerson, D. & Banfield, J. 2009. Iron Oxyhydroxide Mineralization on Microbial Extracellular Polysaccharides. Geochimica et Cosmochimica Acta, 73(13) 3807.

Childs, C. 1992. Ferrihydrite: A review of structure, properties and occurrence in relation to soils. Pflanzen. Bodenk. 155: 441.

Chubar, N., Gerda, V., Szlachta, M. 2014. Mechanism of Selenite Removal by a Mixed Adsorbent Based on Fe-Mn Hydrous Oxides Studied Using X-ray Absorption Spectroscopy. Environ. Sci. Technol. 48(22): 13376-13383.

Coker, V., Byrne, J., Telling, N., Van Der Laan, G., Lloyd, J., Hitchcock, A., Wang, J. , Pattrick R. 2012. Characterisation of the dissimilatory reduction of Fe(III)-oxyhydroxide at the microbe – mineral interface: the application of STXM–XMCD. Geobiology 10(4): 347-354.

Cornell, R., Schwertmann, U. 2003. The iron oxides: structure, properties, reactions, occurrences and uses. Wiley–VCH, Weinheim, Germany.

Czekalla, C., Mevius, W., Hanert, H. 1985. Quantitative Removal of Iron and Manganese by Microorganisms in Rapid Sand Filters (in Situ Investigations). Water Supply, 3(1): 111.

de Vet, W., van Loosdrecht, M., & Rietveld, L. 2012. Phosphorus Limitation in Nitrifying Groundwater Filters. Water Research, 46(4): 1061.

de-Bashan L., Bashan Y. 2004. Recent advances in removing phosphorus from wastewater and its future use as fertilizer (1997-2003). Water Res 38(19): 4222-46.

Del Bubba, M., Arias, C., Brix, H. 2003. Phosphorus adsorption maximum of sands for use as media in subsurface flow constructed reed beds as measured by the Langmuir isotherm. Water Research 37: 3390–3400.

Dhar, R., Zheng, Y., Rubenstone, J., van Geen, A. 2004. A rapid colorimetric method for measuring arsenic concentrations in groundwater. Analytica Chimica Acta 526(2): 203–209.

Dixit, S., Hering, J. 2003. Comparison of arsenic(V) and arsenic(III) sorption onto iron oxide minerals: Implications for arsenic mobility. Environmental Science & Technology 37(18): 4182-4189.

Duckworth, O., Bargar, J., Sposito, G. 2008. Sorption of Ferric Iron From Ferrioxamine B to Synthetic and Biogenic Layer Type Manganese Oxides. Geochimica et Cosmochimica Acta 72(14): 3371.

Duenas, J., Alonso, J., Rey, A., Ferrer, A. 2003. Characterisation of phosphorous forms in wastewater treatment plants. J. Hazard Mater. 97: 1–3.

Emerson, D. 2012. Biogeochemistry and Microbiology of Microaerobic Fe(II) Oxidation. Biochemical Society Transactions, 40(6): 1211.

Emerson, D., de Vet, W. 2015. The Role of FeOB in Engineered Water Ecosystems: A Review. Journal of American Waterworks Association, 107(1): E47-E57.

Emerson, D., Weiss, J. 2004. Bacterial Iron Oxidation in Circumneutral Freshwater Habitats: Findings From the Field and the Laboratory. Geomicrobiology Journal, 21(6): 405.

Fortin, D., Langley, S. 2005. Formation and occurrence of biogenic iron-rich minerals. Earth Science Reviews 72: 1-19.

Fredrickson, J., Zachara, J., Kennedy, D., Dong. H,, Onstott, T., Hinman, N., Li, S. 1998. Biogenic iron mineralization accompanying the dissimilatory reduction of hydrous ferric oxide by a groundwater bacterium. Geochim Cosmochim Acta 62: 3239–3257.

Freundlich, H. 1906. Concerning adsorption in solutions. Zeitschrift fur Physikalische Chemie-Stochiometrie und Verwandtschaftslehre 57(4): 385-470.

Glasauer, S., Weidler, P., Langley, S., Beveridge, T. 2003. Controls on Fe reduction and mineral formation by a subsurface bacterium. Geochim. Cosmochim. Acta 67: 1277–1288.

Goldberg, S., Sposito, G. 1984. A Chemical Model of Phosphate Adsorption by Soils: Reference Oxide Minerals. Soil Sci. Soc. Am. J. 48: 772-778.

Guibaud, G., van Hullebusch, E., Bordas, F. 2006. Lead and cadmium biosorption by extracellular polymeric substances (EPS) extracted from activated sludges: pH-sorption edge tests and mathematical equilibrium modelling. Chemosphere 64(11): 1955-1962.

Hansel, C., Benner, S., Neiss, J., Dohnalkova, A., Kukkadapu, R., Fendorf, S. 2003. Secondary mineralization pathways induced by dissimilatory iron reduction of ferrihydrite under advective flow. Geochimica et Cosmochimica Acta (67)16: 2977–2992).

Heron, G., Christensen, T., Tjell, J. 1994. Oxidation capacity of aquifer sediments. Environ. Sci. Technol. 28(1): 153−158.

Huang, W., Zhang, Y., Li, D. 2017. Adsorptive removal of phosphate from water using mesoporous materials: A review. Journal of Environmental Management 193: 470-482.

Jaisi, D., Kukkadapu, R., Stout, L., Varga, T., Blake, R. 2011. Biotic and Abiotic Pathways of Phosphorus Cycling in Minerals and Sediments: Insights from Oxygen Isotope Ratios in Phosphate. Environ. Sci. Technol. 45: 6254–6261.

Jambor, J., Dutrizac, J. 1998. Occurrence and constitution of natural and synthetic ferrihydrite, a widespread iron oxyhydroxide. Chem. Rev. 98(7): 2549−2585.

Johnson, D., Pilson, M. 1972. Spectrophotometric determination of arsenite, arsenate and phosphate in natural waters. Anal. Chim. Acta 58: 289–299.

Kang, S., Choo, K., Lim, K. 2003. Use of iron oxide particles as adsorbents to enhance phosphorus removal from secondary wastewater effluent. Separation Science and Technology 38: 3853–3874.

Karageorgiou, K., Paschalis, M., Anastassakis, G. 2007. Removal of phosphate species from solution by adsorption onto calcite used as natural adsorbent. Journal of Hazardous Materials A139: 447-452.

Konhauser, K., Kappler, A., Roden, E. 2011. Iron in microbial metabolisms. Elements 7(2): 89−93.

Kosmulski, M. 2002. The pH-Dependent Surface Charging and the Points of Zero Charge. Journal of Colloid and Interface Science 253(1): 77-87.

Kukkadapu R, Zachara J, Fredrickson J, Kennedy D. 2004. Biotransformation of two-line silica-ferrihydrite by a dissimilatory Fe(III)-reducing bacterium: Formation of carbonate green rust in the presence of phosphate. Geochim Cosmochim Acta 68: 2799–2814.

Kulczycki, E., Fowle, D., Fortin, D., Ferris, F. 2005. Sorption of cadmium and lead by bacteria-ferrihydrite composites. Geomicrobiol. J. 22, 299–310.

Langley, S., Gault, A., Ibrahim, A., Takahashi, Y., Renaud, R., Fortin, D., Clark, I., Ferris, F. 2009. Sorption of strontium onto bacteriogenic iron oxides. Environ Sci Technol 43(4), 1008-14.

Langmuir, I. 1918. The Adsorption of Gases on Plane Surfaces of Glass, Mica, and Platinum. Journal of the American Chemical Society 40(9): 1361-1403.

Lau, P.S., Tam, N.F.Y., Wong, Y.S., 1997. Wastewater nutrients (N and P) removal by carrageenan and alginate immobilized Chlorella vulgaris. Environ. Technol. 18: 945–951.

Lehtola, M., Miettinen, I., Vartiainen, T., Martikainen, P. 2002. Changes in Content of Microbially Available Phosphorus, Assimilable Organic Carbon and Microbial Growth Potential During Drinking Water Treatment Processes. Water Research, 36(15): 3681.

Lerk, C., 1965. Enkele Aspecten van Fe Ontijzering van Grondwater. (Some Aspects of the De-ironing of Groundwater). Doctoral dissertation, Department of Mining Engineering, Technische Hogeschool (University of Technology), Delft, the Netherlands.

Li, B., Pan, X, Zhang,D., Lee, D., Al-Misned, F., Mortuza, M. 2015. Anaerobic nitrate reduction with oxidation of Fe(II) by Citrobacter Freundii strain PXL1-a potential candidate for simultaneous removal of As and nitrate from groundwater. Ecol.Eng. 77: 196-201.

Lovley D. 2006. Dissimilatory Fe(III)- and Mn(IV)-reducing prokaryotes. Prokaryotes: A Handbook on the Biology of Bacteria, Vol 2, 3rd Ed: Ecophysiology and Biochemistry, 635-658.

Lovley, D., 2000. Fe(III) and Mn(IV) reduction. In: Lovley, D.R. (Ed.), Environmental Microbe-Metal Interactions. ASM Press, Washington, DC: 3–30.

Ma, Q., Traina, S., Logan, T., Ryan, J. 1993. In situ lead immobilization by apatite. Environmental Science & Technology 27(9): 1803-10.

Manceau, A. 2011. Critical evaluation of the revised akdalaite model for ferrihydrite. American Mineralogist 96(4): 521-533.

McKnight, D., Wershaw, R., Bencala, K., Zellweger, G., Feder, G. 1992. Humic substances and trace metals associated with Fe and Al oxides deposited in an acidic mountain stream. Sci. Total Environ. 118: 485−498.

Mejia, J., Roden, E., Ginder-Vogel, M. 2016. Influence of Oxygen and Nitrate on Fe (Hydr)oxide Mineral Transformation and Soil. Environ. Sci. Technol. 50: 3580−3588.

Mikutta, C., Mikutta, R., Bonneville, S., Wagner, F., Voegelin, A., Christl, I., Kretzschmar, R. 2008. Synthetic coprecipitates of exopolysaccharides and ferrihydrite. Part I: Characterization. Geochimica et Cosmochimica Acta 72(4): 1111-1127.

Mouchet, P., Magnin, J., Mazounie, P. 1985. Elimination du Fer et du Manganese Contenus Dans les Eaux Souterraines: Problemes Classiques, Progres Recents (Elimination of Iron and Manganese From Underground Waters: Classical Problems and Recent Progress). Water Supply,

3(1): 137.

Myers, J. and Myers, C. 2000. Role of the tetraheme cytochrome Cym A in anaerobic electron transport in cells of *Shewanella putrefaciens* MR-1 with normal levels of menaquinone. J. Bacteriol. 182: 67-75.

Newman, D., Kolter, R. 2000. A role for excreted quinones in extracellular electron transfer. Nature 405: 94-97.

O'Loughlin, E., Traina, S., Sims, G. 2000. Effects of sorption on the biodegradation of 2-methylpyridine in aqueous suspensions of reference clay minerals. Environmental Toxicology and Chemistry 19(9): 2168-74.

O'Loughlin, E., Larese-Casanova, P., Scherer, M., Cook, R. 2007. Green Rust Formation from the Bioreduction of γ –FeOOH (Lepidocrocite): Comparison of Several *Shewanella* Species. Geomicrobiology Journal 24(3-4): 211-230.

Ou, E., Zhou, J., Mao, S., Wang, J., Xia, F., Min, L. 2007. Highly efficient removal of phosphate by lanthanum-doped mesoporous SiO2. Colloids Surf. A 308: 47-53.

Parmar, N., Gorby, Y., Beveridge, T., Ferris, F. 2001. Formation of Green Rust and Immobilization of Nickel in Response to Bacterial Reduction of Hydrous Ferric Oxide. Geomicrobiology Journal 18: 375–385.

Posth, N., Huelin, S., Konhauser, K., Kappler, A. 2010. Size, density and composition of cell-mineral aggregates formed during anoxygenic phototrophic Fe(II) oxidation: Impact on modern and ancient environments. Geochim. Cosmochim. Acta. 74(12): 3476−3493.

Rancourt, D., Meunier, J. 2008. Constraints on structural models of ferrihydrite as a nanocrystalline material. American Mineralogist 93(8-9): 1412-1417.

Rentz J., Turner I., Ullman J. 2009. Removal of phosphorus from solution using biogenic iron oxides. Water Res 43(7): 2029-35.

Rentz, J., Kraiya, C., Luther, G., Emerson, D. 2007. Control of ferrous iron oxidation within circumneutral microbial iron mats by cellular activity and autocatalysis. Environmental Science and Technology 41, 6084–6089.

Roden, E., Sobolev, D., Glazer, B., Luther, G. 2004. Potential for microscale bacterial Fe redox cycling at the aerobic–anaerobic interface. Geomicrobiol. J. 21, 379–391.

Romano, S., Bondarev, V., Kölling, M., Dittmar, T., Schulz-Vogt, H. 2017. Phosphate Limitation Triggers the Dissolution of Precipitated Iron by the Marine Bacterium Pseudovibrio sp. FO-BEG1. Front. Microbiol. 8: 364.

Saad, R., Belkacemi, K., Hamoudi, S. 2007. Adsorption of phosphate and nitrateanions on ammonium-functionalized MCM-48: effects of experimental conditions. J. Colloid Interface Sci. 311: 375-381.

Sancey, B., Trunfio, G., Charles, J., Minary, J., Gavoille, S., Badot, P., Crini, G. 2011. Heavy metal removal from industrial effluents by sorption on cross-linked starch: Chemical study and impact on water toxicity. J. Environ. Manage. 92(3): 765-72.

Sarkar, A., Biswas, S., Pramanik, P. 2010. Design of a new nanostructure comprising mesoporous ZrO2 shell and magnetite core and study of its phosphate ion separation efficiency. J. Mater. Chem. 20: 4417-4424.

Schwertmann, U, Fetcher, H. 1982. The point of of zero charge of natural and synthetic ferrihydrites and its relation to adsorbed silicate. Clay Minerals 7(4): 471-476.

Schwertmann, U. 1991. Solubility and dissolution of iron-oxides. Plant Soil 130(1–2): 1–25.

Seder-Colomina, M., Morin, G., Benzerara, K., Ona-Nguema, G., Pernelle, J., Esposito, G., van Hullebusch, E. 2014. *Sphaerotilus natans*, a Neutrophilic Iron-Related Sheath-Forming Bacterium: Perspectives for Metal Remediation Strategies. Geomicrobiology Journal 31(1): 64-75.

Shimizu, M., Zhou, J., Schroder, C., Obst, M., Kappler, A., Borch, T. 2013. Dissimilatory Reduction and Transformation of Ferrihydrite-Humic Acid Coprecipitates. Environ. Sci. Technol. 47: 13375–13384.

Stookey, L. 1970. Ferrozine- a new spectrophotometric reagent for iron. Anal. Chem 42(7): 779–781.

Stratful, I., Brett, S., Scrimshaw, M., Lester, J., 1999. Biological phosphorus removal, its role in phosphorus recycling. Environ. Technol. 20: 681–695.

Straub, K., Benz, M., Schink, B. 2001. Iron metabolism in anoxic environments at near neutral pH. FEMS Microbiol. Ecol. 34: 181-186.

Stumm, W. 1993. Aquatic Colloids as Chemical Reactants: Surface Structure and Reactivity. Colloids and Surfaces A: Physicochemical and Engineering Aspects, 73:1.

Stumm, W., Morgan, J. 1996. Aquatic Chemistry: Chemical Equilibria and Rates in Natural Waters, 3rd edition. Wiley- Interscience, New York, NY, p. 1040.

Suzuki, T., Hashimoto, H., Itadani, A., Matsumoto, N., Kunoh, H., Takada, J. 2012. Silicon and Phosphorus Linkage With Iron Via Oxygen in the Amorphous Matrix of Gallionella ferruginea Stalks. Applied and Environmental Microbiology 78(1): 236.

Tamura, H., Kawamura, S., Hagayama, M. 1980. Acceleration of the Oxidation of Fe2+ Ions by Fe(III)-Oxyhydroxides. Corrosion Science, 20(8–9): 963-971.

Tanada, S., Kabayama, M., Kawasaki, N., Sakiyama, T., Nakamura, T., Araki, M., Tamura, T. Removal of phosphate by aluminum oxide hydroxide. J. Colloid Interface Sci. 257: 135.

University of Washington, "Adsorption Equilibrium Principles" slide deck. [online] available: http://faculty.washington.edu/markbenj/CEE483/Adsorption%20Equil%20Principles_483.ppt

Vrouwenvelder, J., Beyer, F., Dahmani, K., Hasan, N., Galjaard, G., Kruithof, J., & van Loosdrecht, M. 2010. Phosphate Limitation to Control Biofouling. Water Research, 44(11): 3454-3466.

Vuong, T., Monson, P. 1998. Surface Roughness Effects in Molecular Models of Adsorption in Heterogeneous Porous Solids. Langmuir 14(17): 4880–4886.

Yebra, D., Kiil, S., Johansen, K. 2004. Antifouling technology- past, present and future steps toward efficient and environmentally friendly antifouling coatings. Progress in Organic Coatings 50(2): 75–104.

Zachara J., Kukkadapu R., Fredrickson J., Gorby Y., Smith S. 2002. Biomineralization of poorly crystalline Fe(III) oxides by dissimilatory metal reducing bacteria (DMRB). Geomicrobiol. J. (19): 179–207.

Zhang, H., Fang, W., Wang, Y., Sheng, G., Xia, C., Zeng, R., Yu, H., 2013. Species of phosphorus in the extracellular polymeric substances of EBPR sludge. Bioresour. Technol. 142(0): 714-718.

Appendix

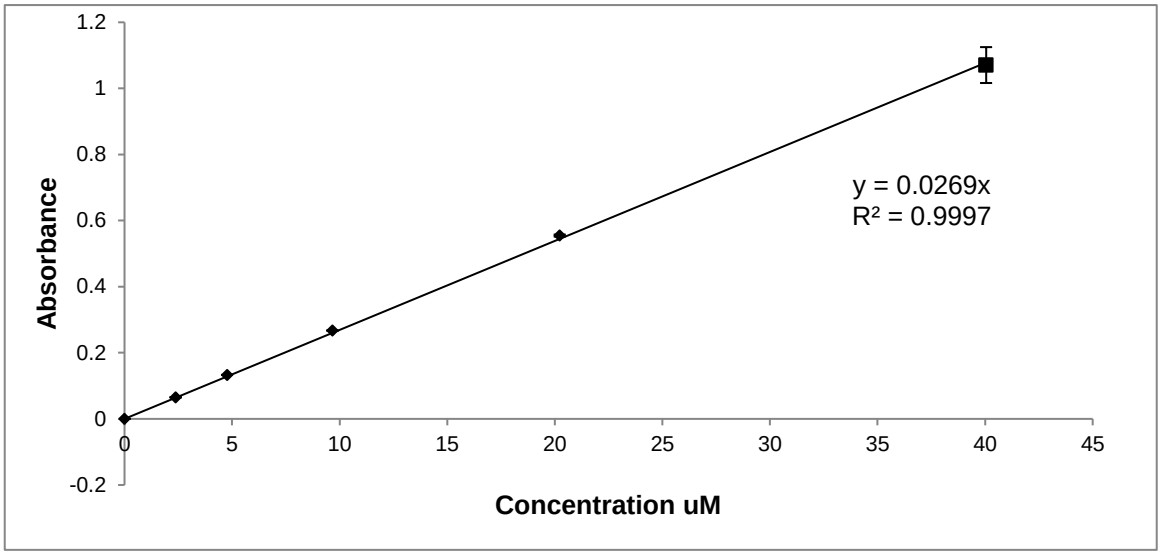

Figure A1. Standard ferrozine calibration curve constructed using samples of known ferrous iron concentration. The linear equation determined from the line of best fit allows the determination of iron concentration in experimental samples.

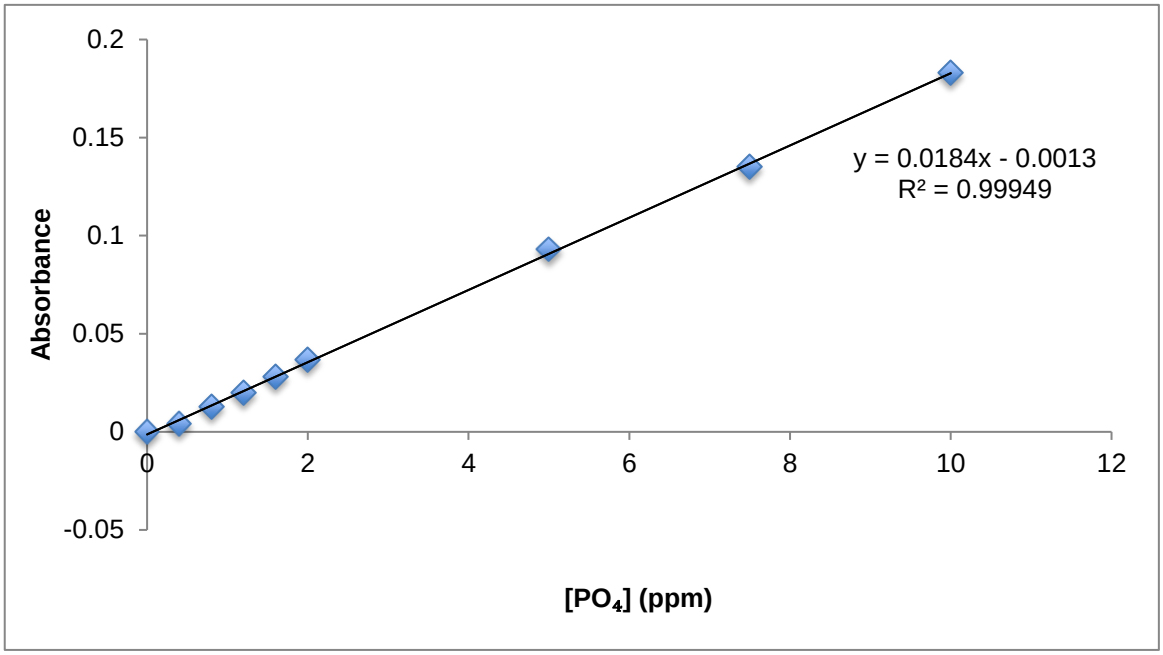

Figure A2. Standard molybdenum blue calibration curve constructed using samples of known phosphate concentration. The linear equation determined from the line of best fit allows the determination of phosphate concentration in experimental samples.

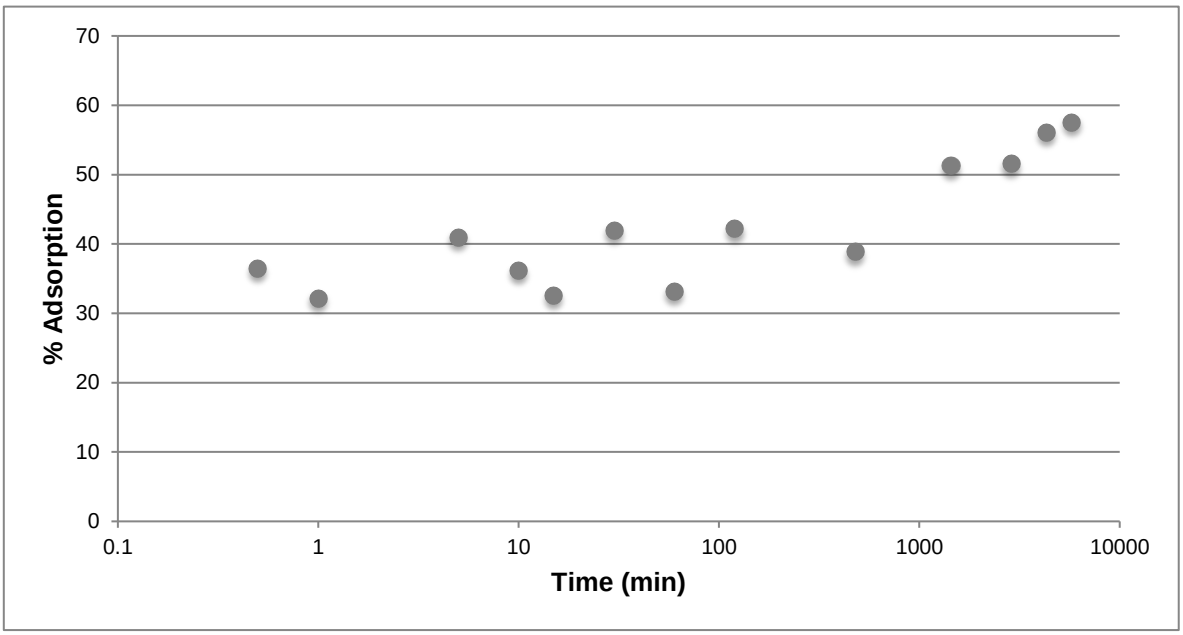

Figure A3. Kinetic adsorption experimental data showing the percentage of phosphate adsorption to the surface of suspended iron oxide particles over time. The x-axis is displayed as a logarithmic scale.

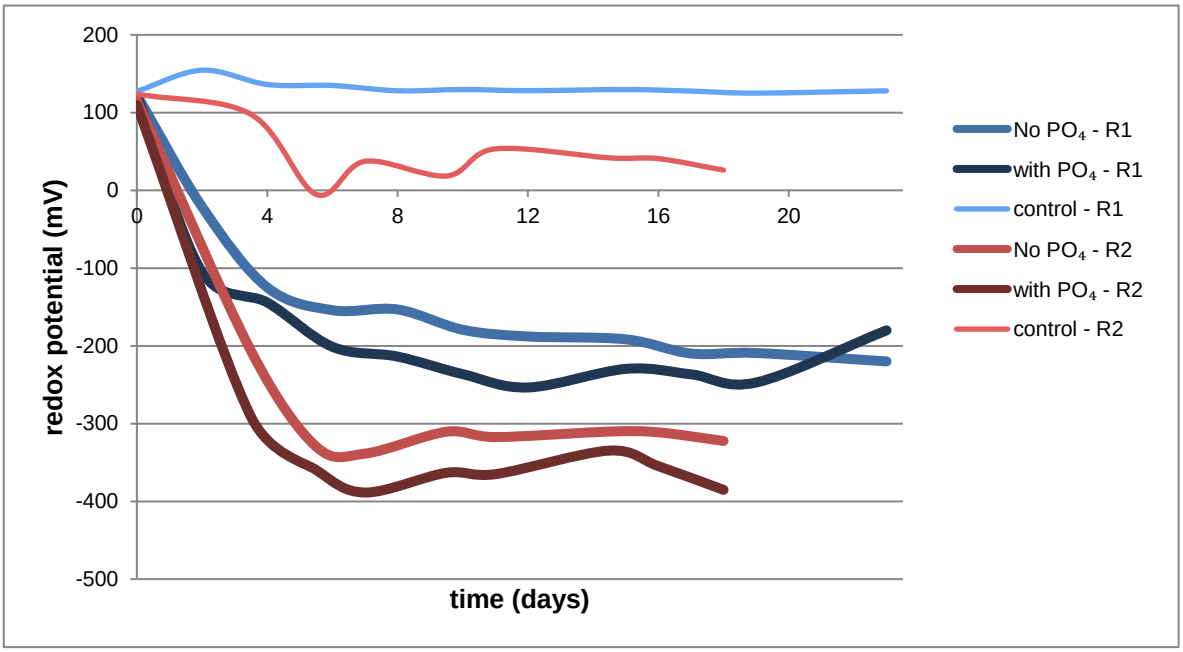

Figure A4. Changes in redox potential over time during reduction experiments. Trials with pure ferrihydrite are shown in blue (R1), and trials using 10% C co-precipitate are in red (R2). Trials with pre-adsorbed phosphate are indicated by the darker lines. The controls (no bacteria) are indicated by the pale, thin lines.

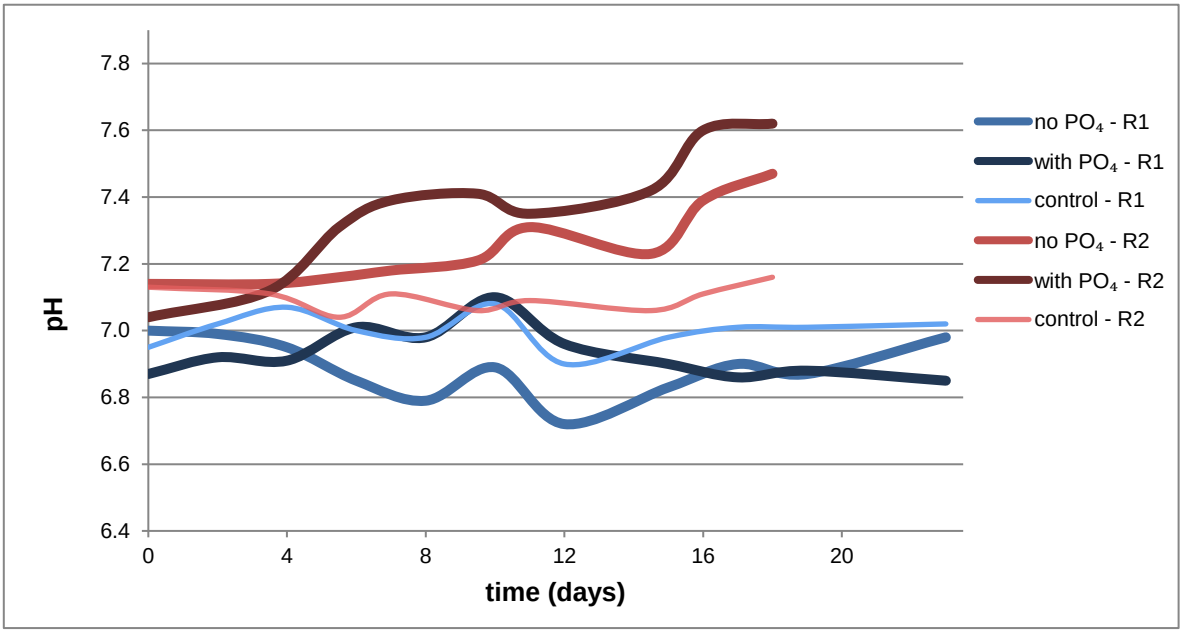

Figure A5. Changes in pH over time during reduction experiments. Trials with pure ferrihydrite are shown in blue (R1), and trials using 10% C co-precipitate are in red (R2). Trials with pre-adsorbed phosphate are indicated by the darker lines. The controls (no bacteria) are indicated by the pale, thin lines.

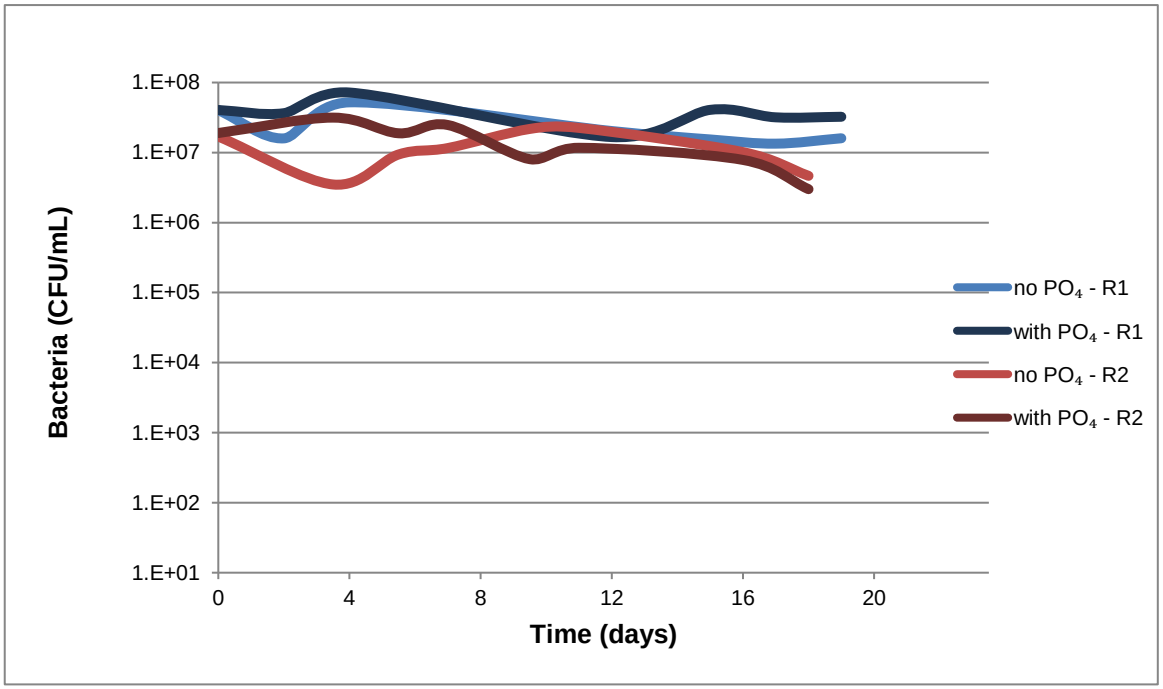

Figure A6. Changes in levels of bacteria, measured in colony-forming units (CFU) per mL, over time during reduction experiments. Trials with pure ferrihydrite are shown in blue (R1), and trials using 10% C co-precipitate are in red (R2). Trials with pre-adsorbed phosphate are indicated by the darker lines. Controls contained no bacteria so are not represented in this figure.

Table A1. Composition of chemically defined medium (CDM) used in reduction experiments.

Ingredient	**Final concentration in medium (M)**
Fumarate	10×10^{-3}
Sodium lactate	10×10^{-3}
NH_2Cl	2.2×10^{-3}
KCl	1.2×10^{-3}
$CaCl_2$	0.61×10^{-3}
NaH_2PO_4-H_2O	3.9×10^{-3}
PIPES buffer (pH 7.0)	4.5×10^{-3}
Nitrilotriacetic acid	7.1×10^{-5}
$MgSO_4$-$7H_2O$	1.1×10^{-4}
NaCl	1.5×10^{-4}
$MnSO_4$-H_2O	2.7×10^{-5}
$ZnCl_2$	8.6×10^{-6}
$FeSO_4$-$7H_2O$	3.2×10^{-6}
$CaCl_2$-$2H_2O$	6.1×10^{-6}
$CoCl_2$-$6H_2O$	3.8×10^{-6}
Na_2MoO_4-$2H_2O$	9.3×10^{-7}
$NaWO_4$-$2H_2O$	6.8×10^{-7}
$NiCl_2$-$6H_2O$	9.1×10^{-7}
$CuSO_4$-$5H_2O$	3.6×10^{-7}
$AlK(SO_4)$-$12H_2O$	1.9×10^{-7}
H_3BO_3	1.5×10^{-6}